DESIGN OF MINIATURIZED COIL SYSTEM USING MEMS TECHNOLOGY FOR EYE MOVEMENT MEASUREMENT

Anurag Umraiya

Department of Electrical and Computer Engineering

McGill University, Montreal

August, 2009

A Thesis Submitted to McGill University in Partial Fulfillment of the

Requirements of the Degree of

Master of Engineering

ABSTRACT

Application of eye movement measurement is especially significant in Neuroscience. Results from eye tracking can give valuable insight into the correlation between neural activity and eye movements. Abnormalities in the eye movements also provide information regarding diagnosis and progress of neurological diseases such as dementia. Another application is in developing human-computer interfaces as a means of communication for the severely handicapped.

Although there are numerous eye tracking techniques available, the magnetic search coil method has been prominently used by researchers due to its high accuracy and precision. This technique typically requires the subjects head to be fixed for accurate measurements due to the use of large field coils. Here we propose a miniaturized coil system using MEMS technology for application in eye movement measurement. The coils were designed and modeled using CoventorWare and MagNet software. The microcoils were then fabricated in the McGill Nanotools microfabrication laboratory. We present the results for using the materials Indium Tin Oxide (ITO) and Aluminium for the fabrication of coils. We found that the resulting coil system is capable of identifying displacements along the X, Y and Z axis. The resolution of the system depends on the configuration of the system, it was calculated to be around 20-40 μm on the plane of the coil and it increases near the centre of the coil. Although the proposed coil system holds significant potential, but further exhaustive testing needs to be performed in an environment simulating eye movements.

RÉSUMÉ

O Mesurer avec précision les mouvements oculaires constitue un élément essentiel dans ledomaine de la neuroscience. Par exemple, capter les mouvemets de l'oeil contribue à la compréhension de la relation entre les activités neuronales et le comportement oculaire. De meme, les irrégularités observées dans les mouvements des yeux aident à diagnostiquer et à surveiller le progrès de plusieurs troubles mentaux comme la démence. En plus, le tracement de la trajectoire oculaire peut être utilisé pour construire des interfaces homme-machine pour les personnes sévèrement handicapées.

Bien que plusieurs techniques de tracement oculaire existent déjà, la bobine de recherche magnétique est fortement utilisée par les chercheurs. Elle offre une haute exactitude et une très bonne précision de mesure. La technique traditionnelle exige l'utilisation de grandes bobines de champs, nécessitant ainsi que la tête du sujet soit fixée en tout temps. En revanche, on propose l'utilisation d'un système de bobines miniaturisées construit avec la technologie MEMS. Les bobines ont été conçues à l'aide des logiciels CoventorWare et MagNet. Les micro-bobines ont été fabriquées dans le laboratoire de micro-fabrication Nanotools de l'Université McGill. On présente les résultats obtenus en utilisant des micro-bobines construites avec la solution solide de l'oxyde de l'étain et l'oxyde de l'indium (ITO). Le système de micro-bobine est capable d'identifier les déplacements dans les trois dimensions X, Y, et Z. La résolution du système dépend de la configuration utilisée. On a trouvé que la résolution peut être entre 20 et 40 μm. Le système proposé est très promettant mais plusieurs tests exhaustifs deraient encore être

appliquées dans des environnements qui simulent de vrais mouvements oculaires.

ACKNOWLEDGEMENTS

First of all, I would like to express my gratitude to my supervisor Prof. Wissam Musallam for his invaluable guidance, kindness and support throughout this study. This thesis would not have been possible without his constructive feedback, suggestions and most of all, his belief in the study.

I would also like to thank the technical team from the McGill Nanotools-Microfabrication laboratory especially Mr. Pierre Huet and Mr. Matthieu Nannini for their assistance during the fabrication process.

INDEX

LIST OF TABLES

LIST OF FIGURES

1 Introduction

There are a wide variety of applications which rely on accurately measuring eye movements [1]. In the field of science, the application of eye tracking is most significant in Neuroscience and Psychology. For studies in attentional neuroscience it is often required to correlate the eye movement with brain activity. In these, usually neural behaviour is recorded along with the eye movements when the subjects respond to different visual stimulus. Some of the experiments might consist of visual fixation on an object, memory tasks and associative tasks. Snodderly et al [2] used an image eye tracker to record the position of a monkey's eye when fixating a light-emitting diode for 5 seconds. Asaad et al [3] trained two rhesus monkeys to perform different tasks such as to associate a visual stimulus with a saccade either to the right or left. Saccades refer to the rapid jerking movement of the eyes. These studies were then used to identify the areas of the brain responsible for different actions and tasks.

Another renowned application of eye tracking is in the experiments involving visual attention such as during reading. Rayner [4] reviewed the work on measuring eye movements for different reading experiments. Eye movements have been proven to be vital for the acquisition of visual information during complex visual-cognitive tasks. Hence other areas such as perception of a scene, art, film have also been a focus of experiments. These studies usually involve studying of eye movement behaviour of patients with a visual impairment such as scotoma. Research scientists have also reported on eye-

movement behaviour while subjects performed natural tasks in a free environment such as making food, playing sports and driving [1].

Accurately measuring eye movements is important for many neuroscience experiments and for the diagnosis of many diseases [5]. Abnormalities pertaining to the spontaneous eye movements can give an indication of a disease progression. Disorders and diseases such as muscular dystrophy, dementia, myopathy and cerebellar ataxia can be better understood with the study of eye movements. Rucker et al [6] were able to measure abnormalities of saccades in patients suffering from late-onset Tay-Sachs disease (LOTS). This provides a means to evaluate the effectiveness of treatments proposed for the disease. Eye movement measurement also provides the opportunity to study human behaviour such as the ability of free will while the subjects respond to visual stimulus [5]. Tanaka and Lisberger [7] studied sites in the frontal cortex of the brain when the monkeys were tracking a moving visual stimulus. The authors were able to identify areas of the brain responsible for smooth eye movements while they fix their gaze on a stationary or a moving spot of light. This was done by measuring eye movements using search coils and associating them with brain activity.

An interactive application of eye tracking is in the field of human-computer interaction. Jacob [8] [1] first introduced an eye-based interactive system which could be used instead of a mouse pointer. Similar systems for the purpose of eye-based typing were further developed which enabled severely handicapped people to communicate by using their eyes. These systems

typically present the user with a virtual keyboard where they could choose letters to be typed by gazing at it for a certain minimum amount of time. Other applications of eye tracking have also been reported in the fields of aviation, advertisement placements and website design [1].

Considering the significance of studying eye movements, numerous measurement technologies have been developed over the last few decades. One of these techniques based on the scleral search coil method is known for its accuracy and high resolution. Typically, a search coil mounted on a contact lens is placed into a patient's eye seated in a structure capable of generating alternating magnetic fields. The induction voltage generated in the coil is used to measure horizontal, vertical and torsional eye movements. These systems require subjects to be head-fixed to constrain the eye movements in a field generated by the coil. Here, we propose a novel method by using a miniaturized coil system fabricated using the Microelectromechanical systems (MEMS) technology for eye movement measurements in an unconstrained environment. With smaller dimensions of the coil system it might be possible to create a setup which can be attached to the subject's head and hence resulting in free movement during experimentation.

Before discussing the details of this method we provide an overview of the various eye tracking technologies available today. These can be broadly divided into four categories and they involve the use or measurement of: Electro-oculography (EOG), photo-oculography (POG), methods based on

reflected light (usually Infra-red) and scleral contact lens/search coils. Eye movements are usually measured in degrees of visual angle [9] [1].

Electro-oculography

This non-invasive technique is based on the fact that there is a permanent potential difference which exists between the cornea (transparent front part of the eye) and the ocular fundus (the interior surface of the eye) (figure 1). This potential difference sets up an electrical field in the tissue surrounding the eye. Rotation of the eye leads to the rotation of the field vector and hence the eye movements can be detected by measuring the skin's electric potential differences using electrodes placed around the eye [1] [10].

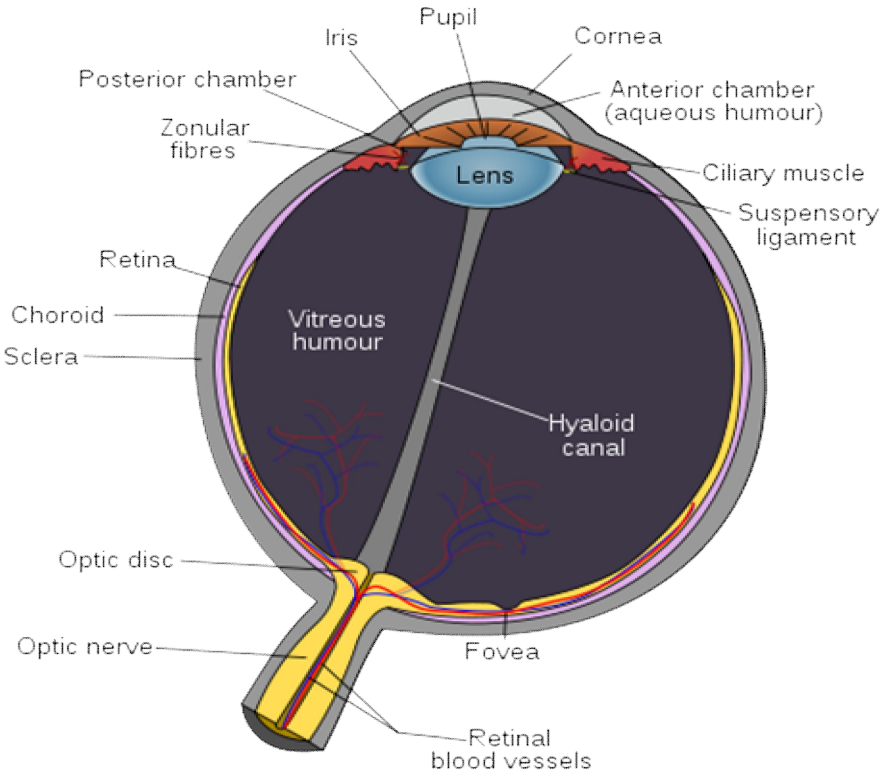

Figure 1: Schematic diagram of the human eye

The resolution of this method is around 1^{o} [10]. This technique is cheap, relatively simple to use and is still used by many clinicians today. However, this has been noted to give spurious signals resulting from metabolic changes in eye and the state of contact between the electrodes and skin. The technique is also quite sensitive to contraction of facial muscles and movement of eyelids. Other disadvantages of this method include difficulties in calibration as well as obtaining vertical movement signal in good quality [9] [1].

Photo-oculography (POG)

This method involves the measurement of distinguishable features of the eyes such as shape of the pupil or position of the limbus (border of the cornea and the sclera) during rotation and translation. This is usually done by extracting the eye position from images of the eye using computer software. This measurement of the ocular features is usually automated. However, the visual inspection of the recorded eye movements might be required, for example, stepping through a videotape frame-by-frame which can be very time-consuming and error prone [1]. The resolution of this technique is around 0.1 degrees with a measurement range of ±30-40 degrees. The sampling rate is limited approximately to 250 Hz [12]. Its temporal resolution is limited by the video recording system's frame rate and the technique is error prone during an eye blink [9]. Another method based on eye images was proposed by Buquet et al [34] where eye images were created by using infrared cameras viewing each eye over a hot mirror. The images were then analyzed by image processors capable of deducing eye movements by using pupil and corneal reflections. They were able to measure relative eye positions to the accuracy

of one degree. This technique was further explored to develop infra-red light based eye tracking methods.

Methods based on reflected light

This method is based on the principle that infra-red light reflected from the eye will vary depending on the eye's position [1] [10]. In some systems images are formed using reflection of the light source from the cornea. These are measured relative to the pupil center and these relative movements are further processed to estimate the eye position. These corneal reflections are also known as Purkinje images [1]. This is a relatively stable method as the apparatus is not disturbed by other light sources. It is capable of providing spatial resolution of 0.1 degrees and a temporal resolution of 4000 Hz [12]. Blinking can cause false measurements as the eye retraction afterwards causes a change in the reflected light. The system is also vulnerable to false measurements caused by head movements [9].

Scleral Search coils

This technique considered to be the most precise eye movement measurement method is the main focus of our study [1]. Coils of wire usually made up of copper are embedded in a modified contact lens. This lens is then placed on the eye using a local anesthetic. Electromagnetic field is generated using field coils placed on the either side of the head and the induced electromotive force (voltage) in the eye coils represents the eye position. This method provides a resolution of about 0.017 degrees for horizontal, vertical and translational motion [10]. As mentioned earlier this method requires the subject's head to

be constrained or the eye would move out of the domain where magnetic field can influence the search coil voltage. Hence the major objective of this study is to explore the possibility of miniaturizing the coil system so that the whole setup can be placed on the subjects head resulting in head-free measurements. As our study is based on this method we hereby describe the techniques developed in the last few decades employing the magnetic search coil measurement principle.

Traditionally magnetic search coils have been favoured for research purposes because of their high spatial and temporal resolution. However, they are invasive which can cause discomfort to the user. Hence other non-invasive methods such as Infrared tracking are sometimes employed instead to measure eye movements. Schmitt et al [15] compared the performance of the two techniques: Infrared eye tracking and Search coils. The results for this study showed that both methods provide similar results. These conclusions are in contrast with results reported from other studies such as by Van Der Geest and Frens [16]. They compared saccadic eye movement measurements utilizing the search coil and infra-red based video-oculography techniques. Schmitt et al did not find the sampling rate of video-based technique (250 Hz) a major influence on the performance while Van Der Geest and Frens had reported that the low sampling rate of video-based technique is a major disadvantage. Traisk et al [17] showed that video based results showed higher variability because of the reduced alertness among the subjects. Schmitt also did not have the problem of slippage of lens during experiments which was observed by other researchers. These dissimilarities in the studies may be attributed to

differences in experimental apparatus and eye tracking algorithms. One commonly observed phenomenon was that the resolution of the search coil method decreases with an increase in displacement. For example rotational displacement smaller than 10 degrees showed a resolution of 0.1 degrees while for larger displacement the resolution dropped to 0.2 degrees [15].

The pioneer study of employing the search coil method to measure eye movement was done by David A. Robinson [13]. The study involved using two magnetic fields in quadrature phase generated by the field coils in the horizontal and vertical directions. There were two pairs of field coils where each pair is used to produce an alternating magnetic field. The four identical circular coils consisted of 80 turns and the width, height of 1 inch. The subject in this experiment was seated with his head and shoulders projecting into an open frame with the dimensions of 2ft x 2ft x 2ft which supported the field coils. The field coils used to generate the horizontal magnetic field were taped to the left and right surfaces of the cube similar to a Helmholtz configuration where they were placed in series along a common axis and separated by a distance approximately equal to the radius of each coil. The field coils for the vertical magnetic field were connected in an identical fashion to the top and bottom of the cube. Two search coils on a lens were placed on the eye and this system was used to measure horizontal, vertical and torsional eye movements. The reported resolution from this method was 15 seconds of arc which is equivalent to 0.0416 degrees. This method was adapted by Fuchs and Robinson to chronically measure eye movement in monkeys [18]. Afterwards other researchers adapted the method and modified the apparatus for their own

experiments. Collewijn et al [19] developed a special flexible ring made of silicone rubber for the purpose of using it for human experiments. The search coil containing nine windings of copper wire of 0.05 mm in diameter was embedded in this ring. Judge et al [20] implanted the search coil in front of extraocular muscles rather than behind them as done by Fuchs and Robinson. This addressed the problem of esotropic strabismus exhibited by animals in the previous studies. Strabismus is the condition in which the eyes are not properly aligned with each other. Remmel [21] further developed an inexpensive eye movement monitor by developing a circuit using components costing less than $300. Kenyon [22] described a coil design to eliminate the need for a corneal anesthetic which was used in previous systems. This design consisted of a magnet wire sandwiched between two soft contact lenses and then adhered to the eye using distilled water.

There have been other variations of the search coil technique to measure eye movements. Kim et al [23] developed a technique to measure eye movements wirelessly. The system consisted of a contact lens with a ring-shaped thin magnet instead of a search coil. Four magnetoresistive sensors were placed on a eyeglasses frame-shaped PCB along with the analog/digital signal processing circuitry. Another technique based on the search coils is the double magnetic induction method (DMI) reported by Reulen and Bakker [24]. In the standard method the electrical wire connecting the eye coil can cause eye irritation and also has been found to frequently break during experimentation. In the technique employed by Reulen and Bakker, a Collewijn coil consisting of a single short-circuited winding is applied to the eye and is placed in the

centre of an alternating uniform magnetic field generated by a Helmholtz configuration. The induced current in the coil generates a secondary magnetic field in quadrature with the main magnetic field. This in turn induces a voltage in a detection coil which is placed in front of the eye and is located parallel to the main magnetic field. The main advantage of this technique is that it allows lead-free eye coil which has been found to cause discomfort in the subjects. The resolution reported by the authors was 0.3 degrees over a range of 40 degrees which is lower than that of scleral search coils. The external coils used in this method have to be adjusted at the beginning of each session and also the whole system is very sensitive to mechanical disturbances. Malpeli [25] described a more stable system utilizing the DMI method by implementing a compensation coil to minimize the undesirable signal prior to amplification. These measures to minimize mechanical disturbances in the DMI method were found to be less inconvenient than dealing with broken coil wires in the standard magnetic-search coil technique.

Bremen et al [26] further compared the performance of the classical scleral search coil (SSC) technique with the one based on the double magnetic induction. They reported similar results as Malpeli and concluded that DMI method works reasonably well despite having a slightly less resolution of 0.3 degrees versus 0.2 degrees for the search coil technique. This DMI system was also found to be very sensitive to mechanical vibrations and required considerable effort to stabilize. One of the other major constraints is that the DMI technique cannot be used to measure eye movements in head-free environments. Ogorodnikov et al [27] developed a system based on the

standard search coil system capable of measuring eye movements in freely moving monkeys. Previous systems used large external coils for the generation of magnetic fields which required the subjects to be head-fixed. Otherwise, head and eye movements would be outside the range of the coil field. In the system developed by Ogorodnikov two orthogonal field coils were placed on the top of the head in a cap which would induce voltage in the coils placed on the eye. The resolution of this system was around 0.2 degrees which was comparable to the standard search coil method results.

In this thesis we explore the possibility of using MEMS technology for eye movement measurement. The method proposed here is based on the already established principle of using search coils for eye tracking. MEMS technology due to its versatility has been at the forefront of advancement in biomedical technology over the recent years. It has allowed the creation of innovative microsystems combining the standard IC fabrication process with biocompatible materials. The possibility of creating microstructures makes MEMS technology an extremely attractive option to explore for the purpose of eye movement detection. Here we explore the option of using optically transparent conductive material Indium Tin Oxide (ITO) for the fabrication of coils. Our aim is to use the inductive link between two or more microcoils to detect the change in position of one. In the subsequent section, design and modeling of the MEMS coil system is presented and discussed. The electromagnetic effects of these coils are analyzed using simulations from CoventorWare and COMSOL software. Simulations performed using the MagNet software to study the effects of different physical parameters of the

coil on the performance are shown. We then provide details on the fabrication procedure for the coil system using the materials Indium Tin Oxide (ITO) and Aluminium. Finally, the results from the testing of the measurement setup using the fabricated coils are discussed.

2 Design and Modeling of the Coils

The functionality depends on the principle of Faraday's law of induction. It states that

$$\epsilon = -d\varphi_B/dt \qquad (1)$$

where ϵ is electromotive force (EMF) in volts and φ_B is the magnetic flux through a circuit. In our setup we use a planar spiral coil to produce an alternating magnetic field which will then further lead to an induced voltage in a secondary circuit/conductor. As the amount of magnetic flux changes upon any relative displacement between the source of magnetic field and the secondary circuit, it will result in a change in the induced voltage. For the application of measuring eye movement, the primary coil used to generate the magnetic field is located close to the eye and a secondary coil or wire placed on the eye itself. The alternating magnetic field from the primary coil will cause an induced voltage in the eye coil. Assuming that there is no relative movement between the eye and the secondary coil, any eye movement will result in a change of this induced voltage in the coil which can be measured. This information can then be further processed to measure the eye movement from its original position. One of the objectives of this study is to minimize the size of the primary coil while maximizing the resolution of the system. We first focus on the design of the coil and to understand the different parameters which can affect its performance.

We need the coils to produce a strong magnetic field while keeping the parameters of the coil to be practical for experimentation. From the literature it has been proven that the circular spiral coil generates a stronger magnetic field when compared to other designs. Ramadan *et al* [28] compared the magnetic field profiles of the spiral design (figure 2) with straight-conductors meander, mesh-shaped meander and the rosette-shaped meander designs. They concluded that the spiral design produces a magnetic field up to five times larger than the other micro-electromagnet designs for the same current and electromagnet area.

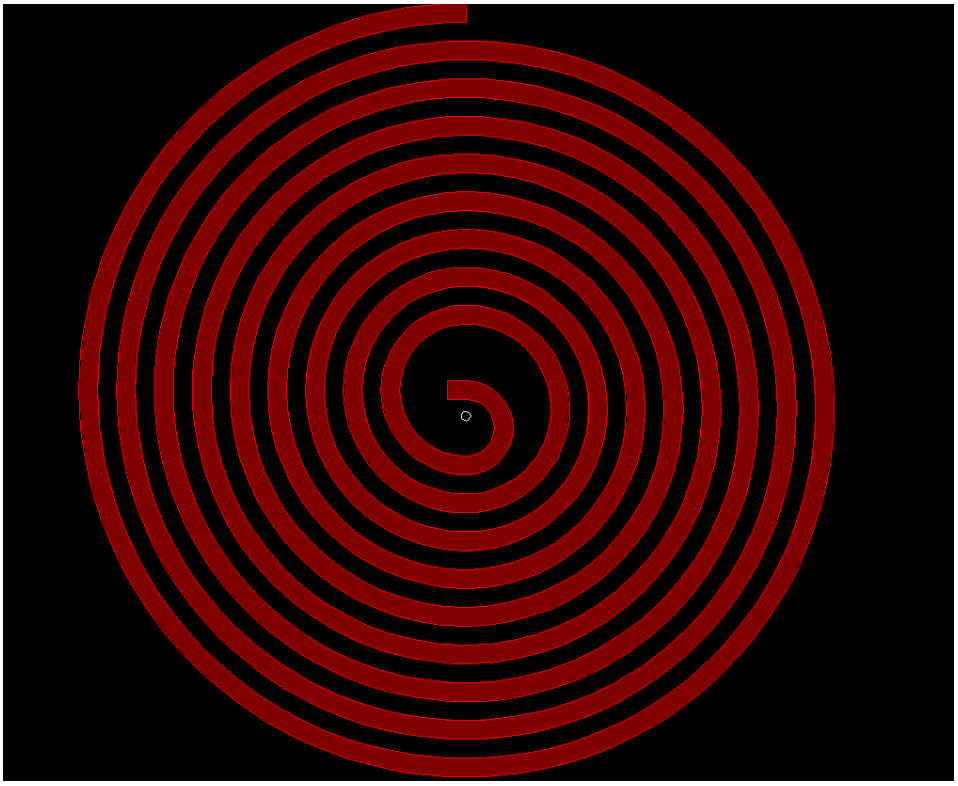

Figure 2: The planar spiral design coil

The circular spiral design has also been proven to have a higher quality factor than the square and octagonal spiral [3]. The quality factor is defined as the following:

$$Q = \frac{\omega L}{R} \qquad (2)$$

It is the ratio of its inductive reactance to the resistance and is a measure of its efficiency. Higher Q means the design is closer to an ideal, lossless inductor. The current components from the different turns in the spiral design sum up to create a strong magnetic field in the centre of the coil. A spiral coil was designed using Coventorware and the following plot was obtained after conducting simulations using the COMSOL multiphysics module software. Figure 3 shows the magnetic field density across the surface of the coil and it can be seen that it is highest at the centre.

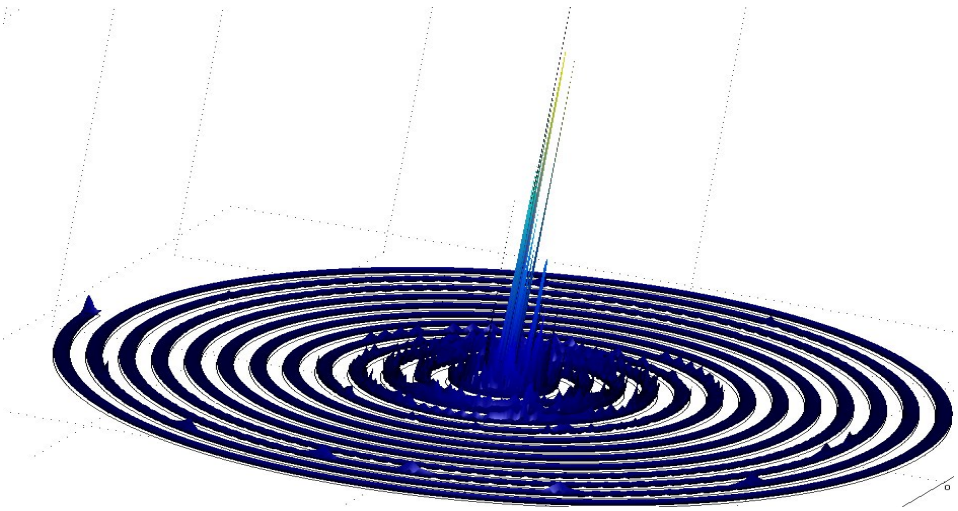

Figure 3: 3D Surface plot of magnetic field density in a spiral coil

The spiral coil can be thought of consisting of N co-axial loops. The summation of the z-components from the N turns is the cause of a stronger

magnetic field in the centre of the coil. The total z-component of the magnetic flux density due to N loops can be calculated as

$$B_z = \sum_{k=0}^{N} \frac{\mu_o I a_k^2}{2(a_k^2 + z^2)^{\frac{3}{2}}} \qquad (3)$$

where I is the current, μ_o is the magnetic permeability and a_k being the radius of the loop. With a strong magnetic field this design would enable the inductive link to function even at larger distances.

One of the main design considerations is to maximize the produced magnetic field as it is directly proportional to the induced voltage. This can be done by increasing the current in the coil but the maximum current is also limited by joule heating. The current has to be within limitations so as not to damage the spiral coil. Consequently, it is better to optimize the geometry of the coil which consists of the physical parameters shown in Figure 4:

N = number of turns

t = thickness of the track

d = distance between tracks

w = width of each track

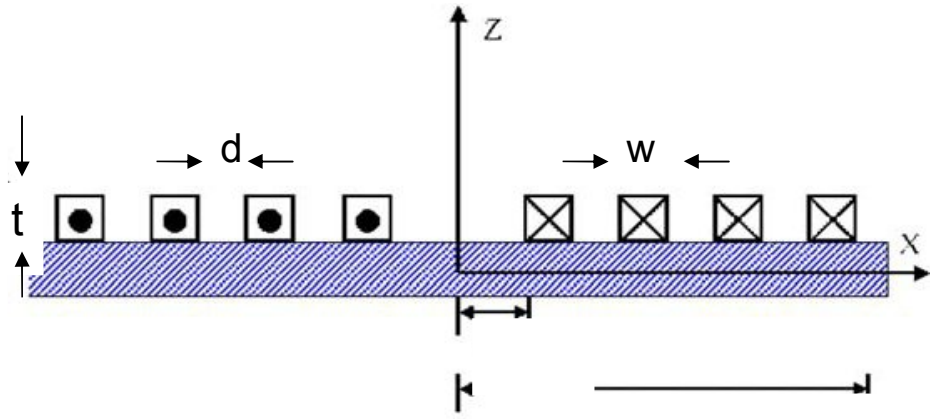

Figure 4: Cross-sectional view of the spiral coil geometry

To understand the significance and effect of these parameters extensive simulations were performed using the software MagNet. The trial 2-D magnetostatic version of the software was used for the simulations.

2.1 Simulations using MagNet

As it is a 2-D environment, we can only model and observe a cross-sectional view of the coils. Here we use two identical coils for the simulations. One of the coils will be used as the primary coil used to generate the magnetic field from a direct current. The other secondary coil is located at a certain vertical distance away from the primary. In the first case we observe the amount of magnetic flux through the secondary coil in the original position. Thereafter, we change the different parameters such as current, distance and others mentioned earlier to study their effects on the magnetic flux through the secondary coil. The amount of magnetic flux through a circuit is directly proportional to the induced voltage and hence affects the performance of the system.

Scenario 1

Here we define the structure of the two coils and also their position with respect to each other. The magnetic flux linkage in the secondary coil in this scenario is then considered as the reference.

Attributes of the Primary coil (bottom cross-section in figure 5):

Number of turns = 6

Width of track = 1 mm

Height of track = 1 mm

Current = 1 A

Attributes of the Secondary coil (top cross-section in figure 5):

Number of turns = 6

Width of track = 1 mm

Height of track = 1 mm

Current = 0 A

Distance between the primary and secondary coil = 5 mm

Note that the simulated coils do not represent the actual dimensions of the microcoils. We decided to use a simpler design with smaller number of turns and with dimensions in millimetres which was more convenient to model in the software. For instance, the actual microcoils with number of turns around 70 led to impractical simulation times. Also, in order to study the effects of different parameters this design was found to be more than adequate.

In the first case both the coils are aligned with each other perfectly as can be seen from figure 5.

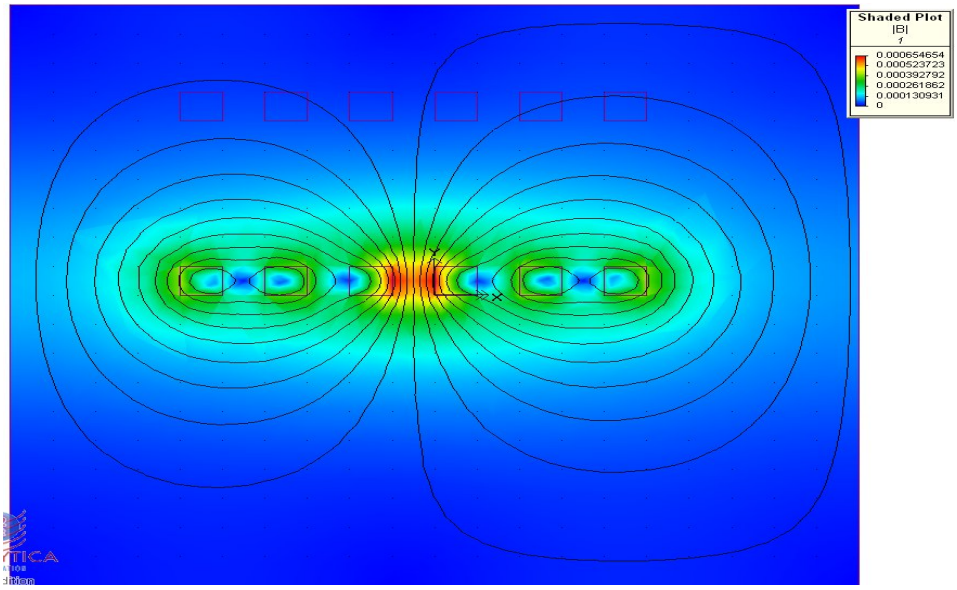

Figure 5: Plot showing magnetic flux lines obtained from MagNet software for Scenario 1

In figure 5 we can see the magnetic flux lines through the two coils. Here we note the flux linkage in the secondary coil. In the subsequent scenarios we change the attributes one by one and analyze the change in magnetic flux linkage. Note that we study these effects by comparing the flux linkage from Scenario 1 only.

Flux linkage in Secondary Coil: 5.03687723777e-010 Wb

Scenario 2

The current in the primary coil was increased to 10 A from 1 A (figure 6).

Flux linkage in Secondary Coil: 5.03687723777e-009 Wb

In this case the flux linkage also increased 10 times in the secondary coil. This is consistent with the theory as current is directly proportional to the magnetic field.

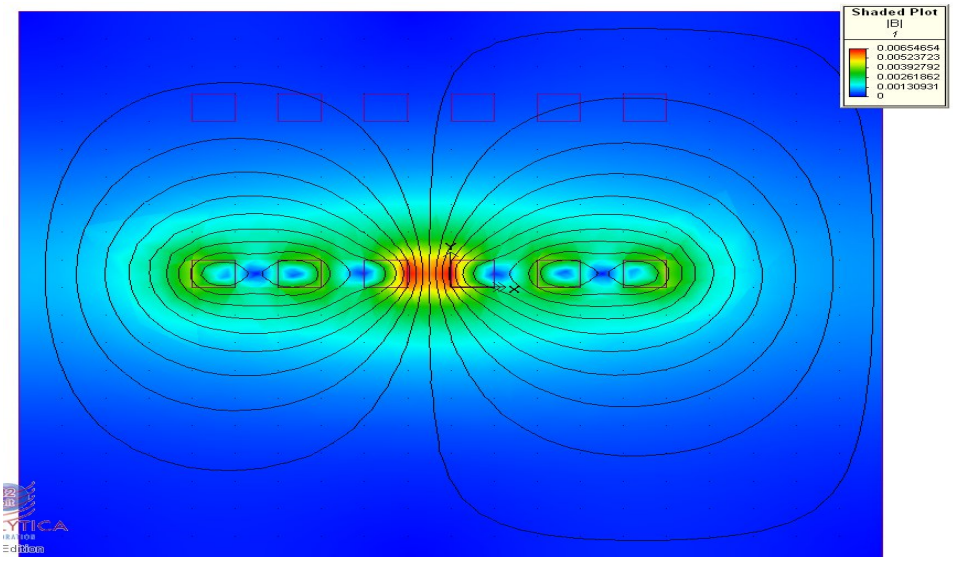

Figure 6: Plot showing magnetic flux lines obtained from MagNet software for Scenario 2

Scenario 3

The distance between primary and secondary coils was reduced from 5 mm to 4 mm (figure 7).

Current in Primary Coil was set back to 1 A as in Scenario 1.

Flux linkage in Secondary Coil: 7.394942843702e-010 Wb

Flux linkage in the secondary coil increases as a larger amount of magnetic flux passes through the area of the coil compared to Scenario 1.

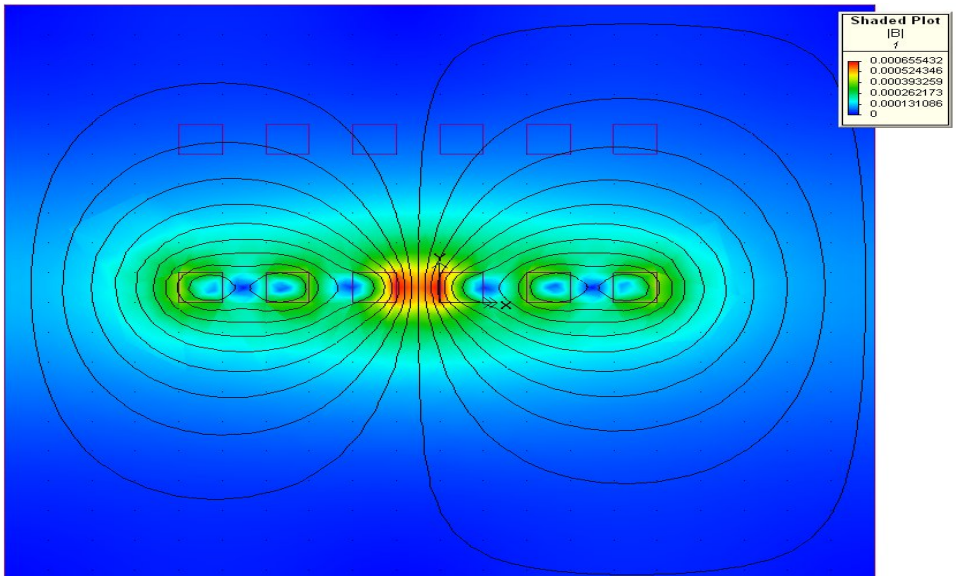

Figure 7: Plot showing magnetic flux lines obtained from MagNet software for Scenario 3

Scenario 4

The thickness of each track in the primary coil was increased to 2 mm (figure 8).

Flux linkage in Secondary Coil: 4.864791875671e-010 Wb

Flux linkage decreases in the secondary coil as the current components producing the magnetic field are located at a further distance.

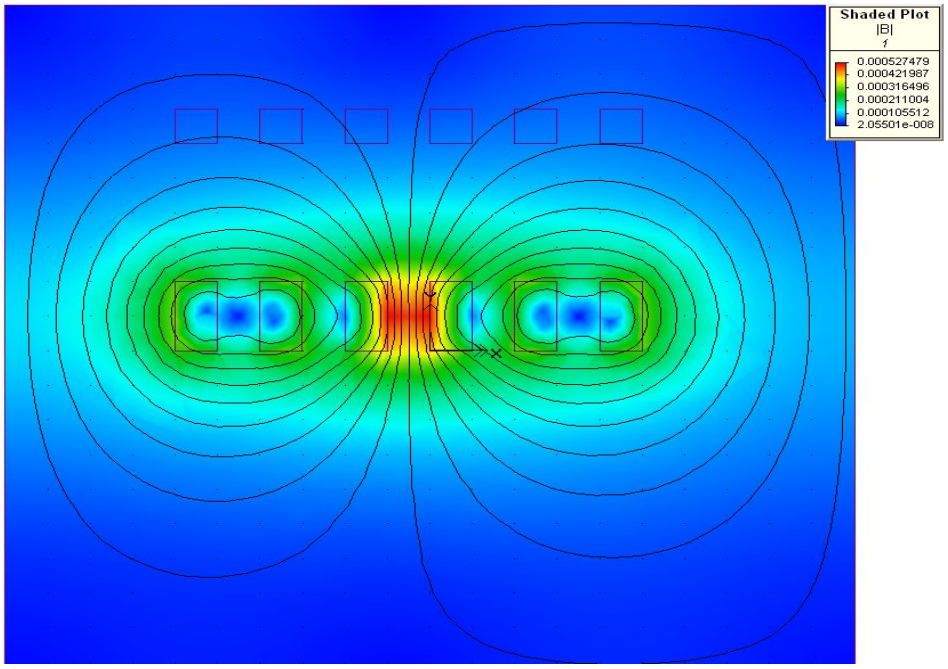

Figure 8: Plot showing magnetic flux lines obtained from MagNet software for Scenario 4

Scenario 5

The distance between the turns for the primary coil was increased from 1 mm to 2 mm (figure 9).

Flux linkage in Secondary Coil: 4.864791875671e-010 Wb

Flux linkage decreases as the current components producing the magnetic field are at a larger distance from the secondary coil.

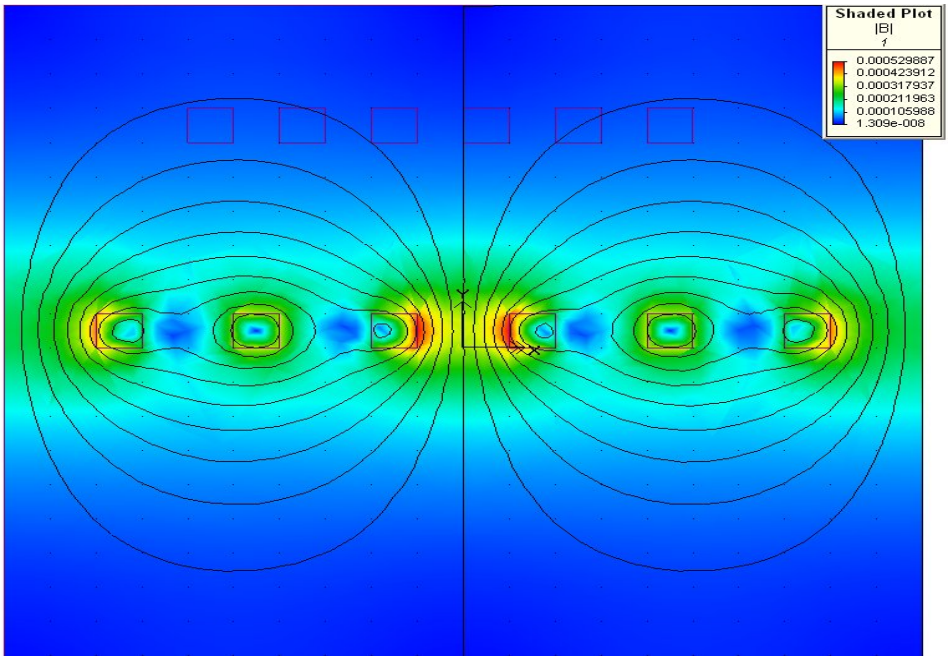

Figure 9: Plot showing magnetic flux lines obtained from MagNet software for Scenario 5

Scenario 6:

The size of the airbox in the solver was increased to accommodate larger coils (figure 10).

Flux linkage in Secondary Coil: 8.843385475357e-010 Wb

In the subsequent scenarios we will compare the flux linkage in the secondary coil with value given above.

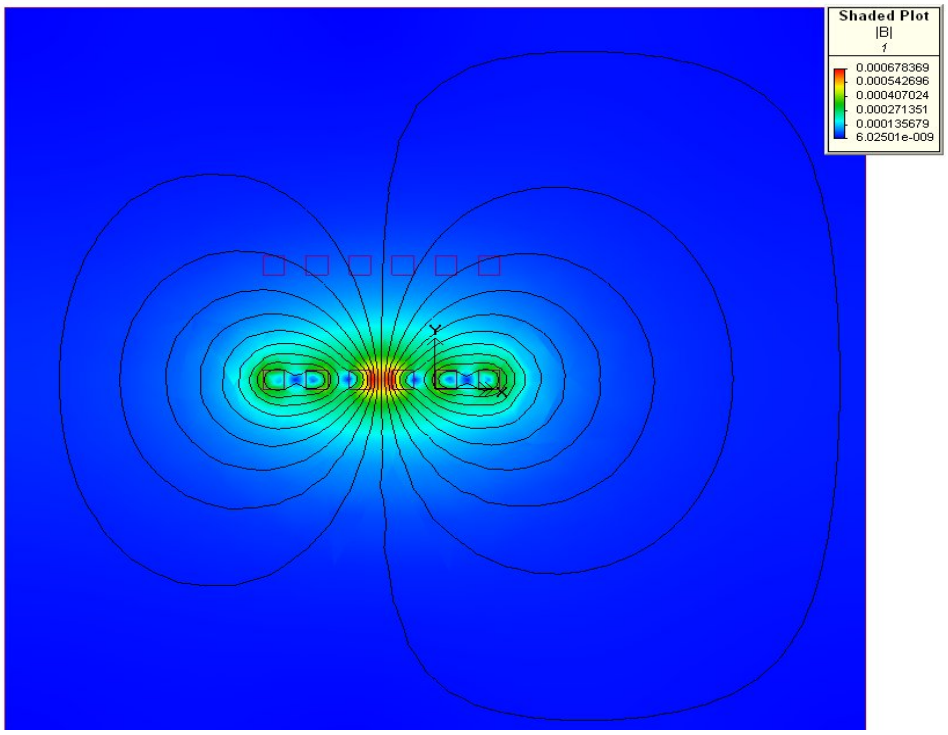

Figure 10: Plot showing magnetic flux lines obtained from MagNet software for Scenario 6

Scenario 7

The number of turns in the primary coil was increased to 8 from 6 in the original case (figure 11).

Flux linkage in Secondary Coil: 1.331733230275e-009 Wb

Flux linkage increases as the number of current components producing the magnetic field has increased.

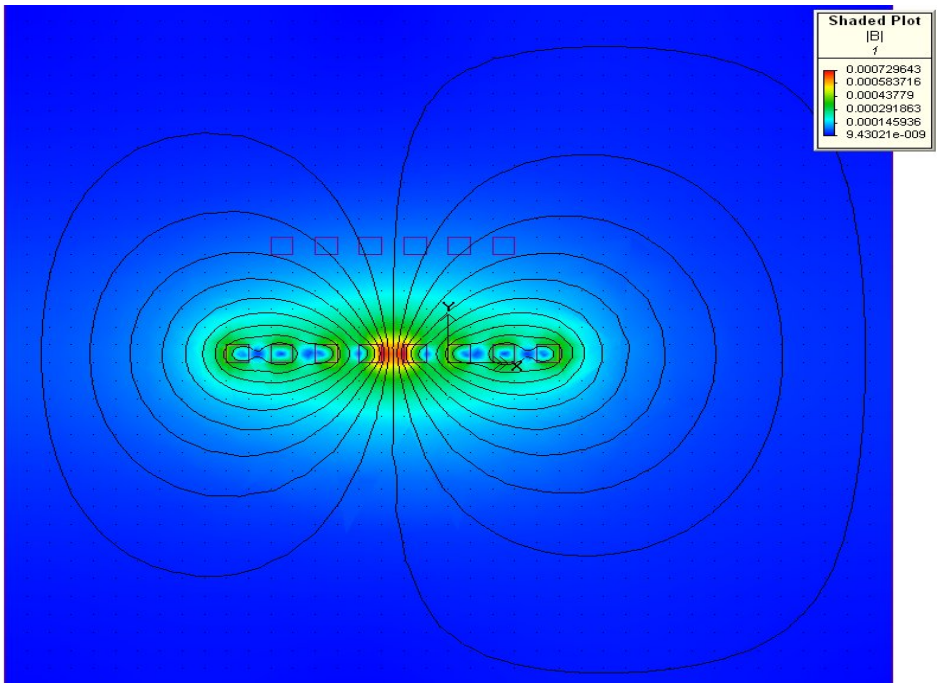

Figure 11: Plot showing magnetic flux lines obtained from MagNet software for Scenario 7

Scenario 8

The number of turns in the secondary coil was increased to 8 from the earlier 6.

Flux linkage in Secondary Coil: 1.331712268308e-009 Wb

Flux linkage increases as the area of the coil increases. It has roughly the same effect as increasing the number of turns in primary coil.

Scenario 9

The secondary coil was displaced by 1 mm in the –x direction (figure 12).

Flux linkage in Secondary Coil: 7.637674087761e-010 Wb

Flux linkage decreases as the coils are not aligned anymore.

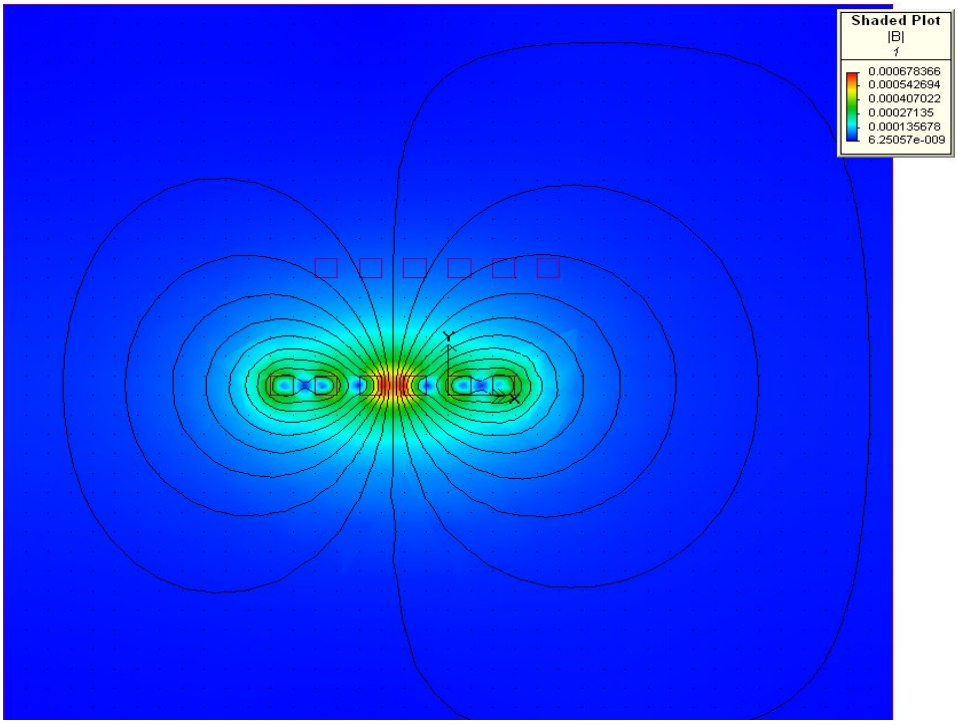

Figure 12: Plot showing magnetic flux lines obtained from MagNet software for Scenario 9

Scenario 10

The secondary coil was displaced by 1 mm in the +x direction.

Flux linkage in Secondary Coil: 7.719773042973e-010 Wb

Similar to Scenario 9 the flux linkage decreases as the coils are not aligned.

We can see from the simulation results that it is important to be careful while designing the spiral coil in order to have the desired results. This information is later used to decide the optimal design. For instance, in order to increase the magnetic flux it is required to decrease the distance between turns of the coils. Alternatively this can also be achieved by decreasing the distance between the two coils or by increasing the number of turns. However, these attributes are also limited by the design and fabrication processes which are discussed later. Although the simulations provide valuable insight to the effects of different

physical attributes of the spiral coil, the exact values of magnetic flux linkage cannot be used for predicting induced voltages. This is because the software used for simulations is strictly confined to modeling 2-D coils using direct current (DC). This oversimplifies the whole system and does not take into account issues such as the skin effect. These can have a significant affect on the electromagnetic induction especially when dealing with alternating currents at high frequencies. However, the simulation results do provide us with valuable information regarding the effect of the physical attributes on the magnetic flux and finally on the induced voltage. Table 1 summarizes the results of the simulations performed using MagNet.

Scenario number	**The applied change in the configuration of coils**	**Effect on flux linkage in Secondary coil**
1	Original Position	5.03687723777e-010 Wb
2	Increasing Current to 10 A	Increases 10 times
3	Decreasing distance between the coils	Increases
4	Increasing thickness of tracks of Primary	Decreases
5	Increasing distance between turns for Primary	Decreases
6	Increasing the size of the airbox for simulations	Increases
7	Increase number of turns in	Increases

	primary	
8	Increase number of turns in Secondary	Increases
9	Displace Secondary 1 mm in the –x direction	Decreases
10	Displace Secondary 1 mm in the +x direction	Decreases

Table 1: Summary of the simulations performed using MagNet software

2.2 Simulations using CoventorWare

The 3-D MEMS designing software CoventorWare was used to model the actual microcoils which were later fabricated and also to perform electromagnetic simulations. In order to achieve the required performance from the system the physical attributes of the microcoil such as the width, thickness and number of turns need to be optimized. While doing so, we have to keep in mind the limitations imposed by the fabrication process and testing equipment. For instance, a track width should not be smaller than 10 μm due to the limitations on the minimum feature size. These issues are discussed in more detail later in the subsequent sections.

Initially, in order to use the microcoils for eye movement measurement, it was decided to use an array of the coils instead of a single secondary coil. We would hereafter refer to this array as the sensor array. This configuration allows for more accurate results as the data from multiple coils can be

analyzed to remove any errors or discrepancies. The configuration remains the same as before and the secondary coil is simply replaced by an array of coils. Movement of the sensor coils alters the coupling between the primary and sensor coils. This movement results in a change in the induced voltage or current in the sensor coils which can be further processed to calculate the displacement of the array coils.

First we provide results from the electromagnetic simulations performed using the MemHenry module of CoventorWare application. The primary coil and the 2 x 4 sensor array coils were designed with a diameter of around 250 μm. The width of each track and the distance between tracks was set to 10 μm. The distance between the primary coil and sensor coils was set to be 300 μm. The primary coil induces current in the array coils and the change in current density is analyzed when the sensor array is displaced with respect to the primary coil. The initial arrangement of the coils can be seen in figure 13. The coloured coil is the one which has current flowing in it. Comparatively the induced current in the sensor coils is quite small.

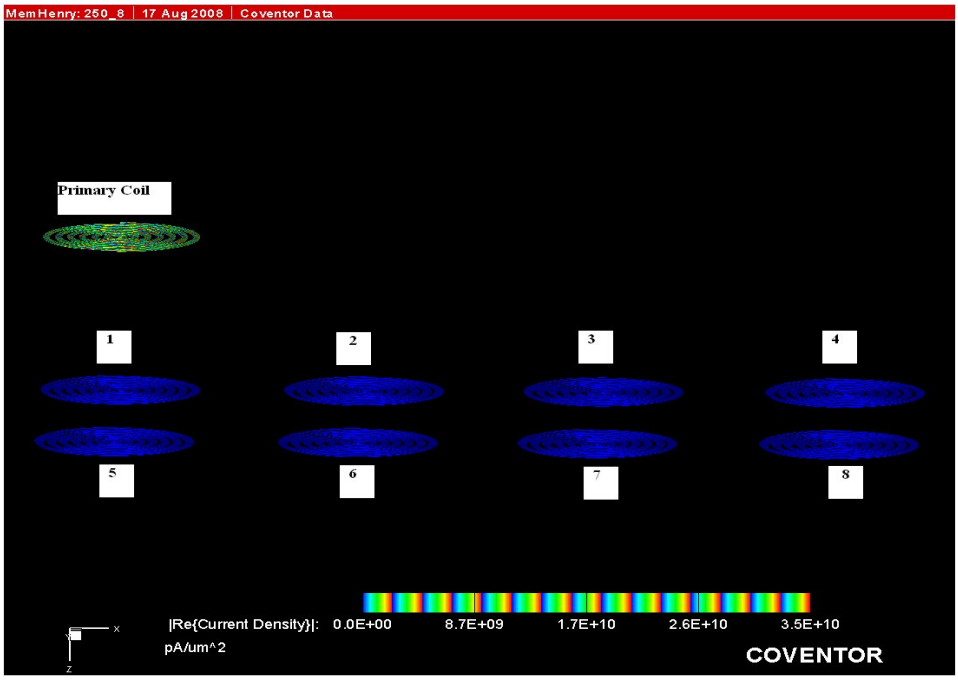

Figure 13: The arrangement consists of primary current carrying coil at the top and sensor coil array at the bottom. The eight coils at the bottom consisting of the array lie in the x-y plane and the primary coil is located at a distance 300 μm in the z-direction

The primary coil remains stationary in all the subsequent cases. The sensor array was displaced to see its effect on the induced current density. In this particular case the current carrying coil is directly in front of sensor coil numbered 1 in the figure 13. The following figure 14 shows the induced current density in the sensor coils. Parts of the coils with higher current density are shown in color in all the subsequent figures.

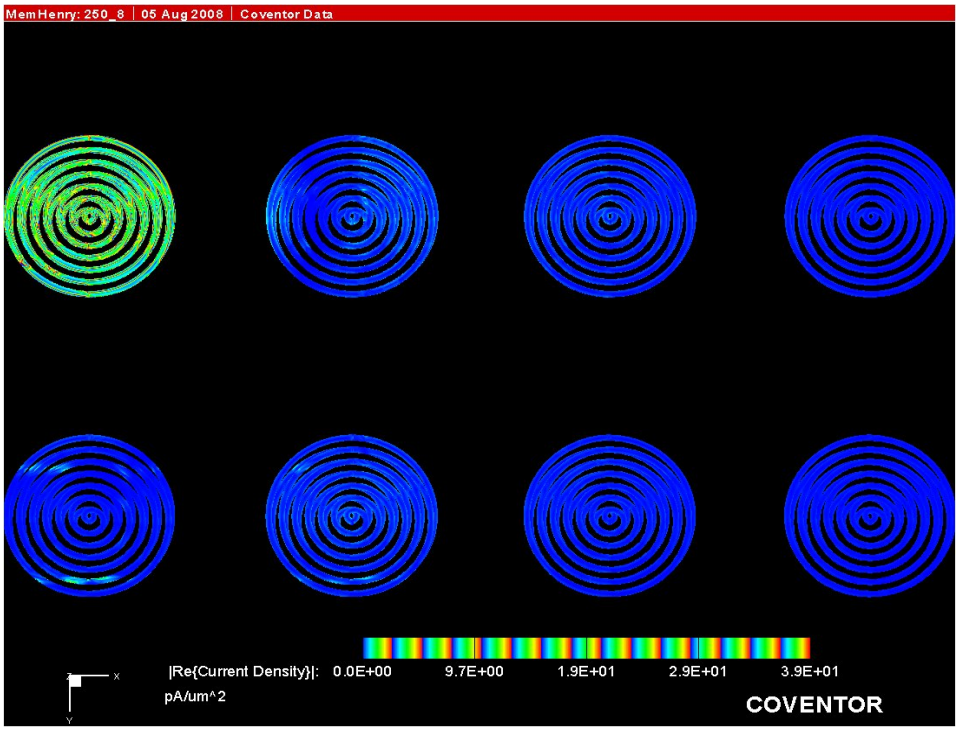

Figure 14: The induced current density in the sensor coils as viewed in the x-y plane. The primary coil is not shown in the figure

Note that the maximum amount of current is induced in the first coil because the primary current carrying coil is placed directly above it. The other coils have negligible induced current. The software uses finite element modeling and the induced current is not uniform on the surface of the coils. All the values for current density were measured in the units of $pA/\mu m^2$. The current density in the first sensor coil was approximately 12621 while it was found to be around 420 in the second one. During testing the induced voltage would be measured across the two ends of the coils instead. These simulations help to verify that this configuration of microcoils can be used to detect motion.

The sensor array is then moved from its previous position as shown in figure 15. Note the change in position of the primary coil and especially the induced current distribution among the sensor coils as compared to figure 14.

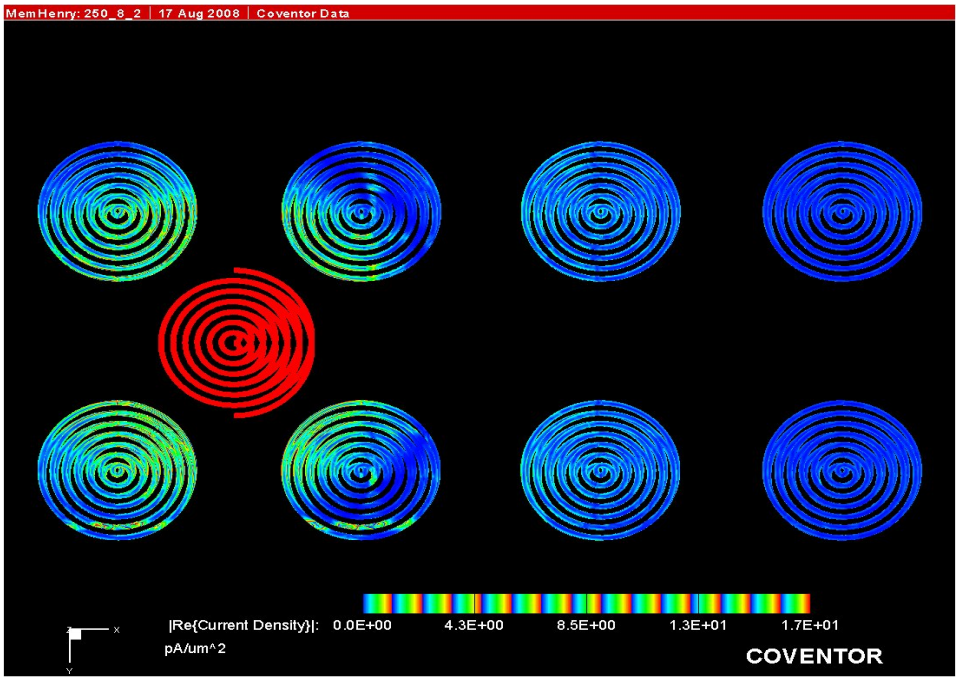

Figure 15: A view from the top of the configuration of the system after the sensor array has moved in both horizontal x and vertical y directions. Primary coil is shown in red color because the current in it is very large compared to the induced current. The induced current density in parts of sensor array coils is also shown.

The primary coil now lies in between the coils 1, 2, 5 and 6 when seen in the x-y plane. It can be observed from figure 15 that the current density in the coils was highest which were in closer proximity to the primary coil. The following table shows the induced current density in the coils 1, 2, 5 and 6 and their distance from the primary coil. These values of current density were taken from the points which were closest to the primary coil.

Sensor Array	Induced Current density ($pA/\mu m^2$)	Distance from the primary coil (µm)
Coil 1	4405	437
Coil 2	4124	444
Coil 5	5080	433
Coil 6	4186	440

Table 2: The induced current density in the sensor coils with the distance

The distance as shown in Table 2 was measured from the centre of the coils to the centre of the primary coil. The current density is highest in the sensor coil which lies at the shortest distance away from the primary coil. Thus we can use the values of induced currents to estimate the position of the sensor coils with respect to the primary coil. This can further be used to deduce the angular displacement of the sensor array.

The following figure 16 shows the arrangement of the coils after the sensor array is further moved to the right in the horizontal x-direction. The primary coil now lies between sensor coils 4 and 8.

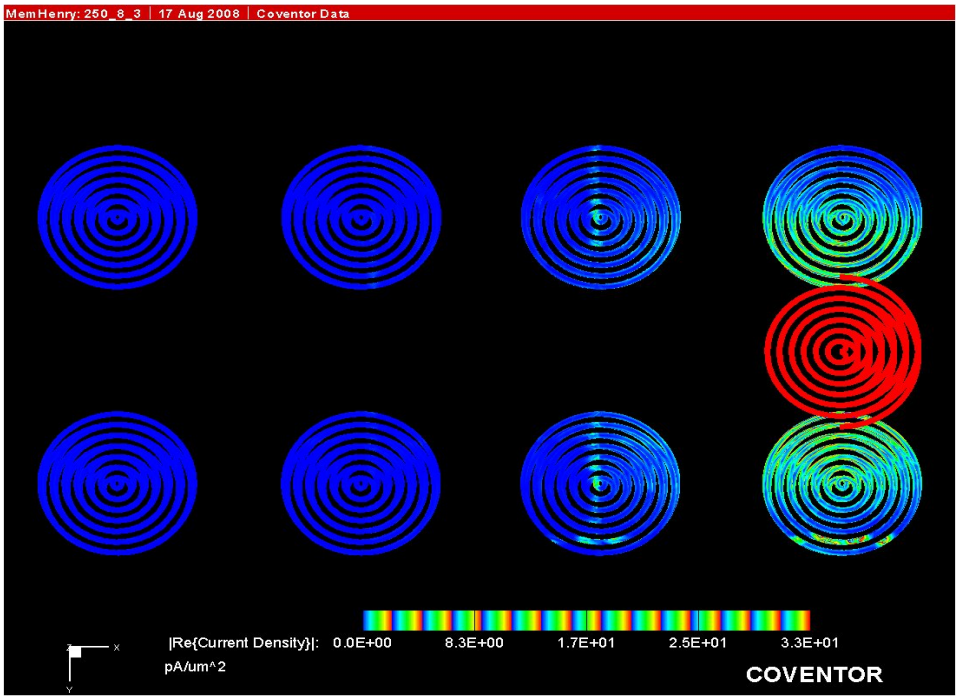

Figure 16: Top view of the configuration after the sensor array has moved in the horizontal direction

The induced current density in the coils 4 and 8 is 4647 and 4683 pA/μm^2 respectively. The current density is almost equal as the primary coil is now equidistant from the two coils. These simulations show that the induced current in the sensor coils changes for every displacement with respect to the primary coil. Hence this current distribution among the sensor coils can be used to find the position of sensor array with respect to the primary coil. The displacement of the sensor array from its previous position can be calculated with this information.

2.3 Modeling of the Microcoils

The masks with the coil patterns were designed using CoventorWare and then these were used to fabricate the coils for testing. In the simulations the minimum resolution for the coils was kept 10 μm as this is limited by the micro fabrication process. This minimum resolution was tested using metals such as Aluminium and Gold. However if the coils are made of these materials and placed on the eye then it would occlude the vision of the subject. Hence it was decided to use Indium Tin Oxide (ITO) instead to fabricate the coils. ITO provides a unique combination of electrical conductivity and optical transparency [30]. The same resolution of 10 μm was not tested in the McGill Nanotools fabrication laboratory for ITO and it was decided to increase the resolution to 25 μm in order to have a safe margin. The thickness of the tracks can be varied during the fabrication process during deposition.

Another restriction imposed by the fabrication process is wire bonding. There are two ends of the spiral coil which need to be connected via micro-wires. Since the wire used for bonding has a diameter of 25 μm it is not feasible to bond it to a track of the same width. Hence square shaped bonding pads were created with dimensions of 100 μm by 100 μm located at the two ends of the spiral (figure 17). The spiral end located near the centre of the coil (Bonding Pad #1) can only be connected with the bonding wire by making a large loop over all the turns of the coil.

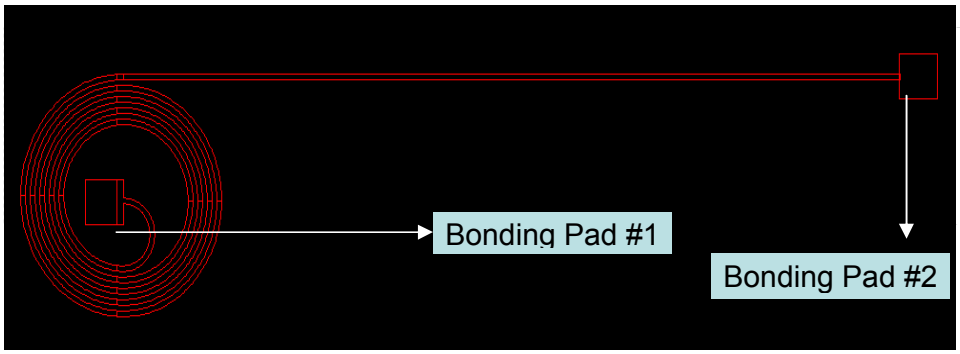

Figure 17: The spiral coil with a diameter of 1mm designed using CoventorWare

Two sets of coils were designed for the fabrication mask; the properties of these are given below.

C1, Diameter = 1 mm

Number of turns N = 10

Distance between tracks, d = 25 µm

Width of tracks, w = 25 µm

C2, Diameter = 7 mm

Number of turns N = 70

Distance between tracks, d = 25 µm

Width of tracks, w = 25 µm

The individual coil designs for C1 and C2 can be seen in figures 17 and 18 respectively. Figure 19 shows the complete layout of the mask design comprising of these coils. The main aim of the project is to create a miniaturized coil system capable of measuring eye movements. The simulations using MagNet and CoventorWare did not provide details for the

specific coil size which would be optimal for this purpose. It is unrealistic to simulate the actual testing environment in software as there are a large number of factors which can affect the functionality of the system. For instance the conductivity and other properties of the fabricated coils can vary significantly depending on the micro-fabrication process. The testing equipment including wires, cables and the actual configuration of the coil system are other factors which can affect the results. The other solution is to actually fabricate coil of different sizes and then test them in a laboratory environment. Hence a small coil of diameter 1 mm and a large coil of diameter 7 mm were designed. As we concluded from the simulations, the number of turns (N), width of each track (w) and distance between tracks (d) directly affect the produced magnetic field. The optimal design is to have the maximum number of turns while minimizing the total area of the coil. This is done by minimizing w and d. The value for these was chosen to be 25 μm instead of the minimum 10 μm due to the lack of a standardized fabrication process using ITO. Increasing this value of the smallest feature size can lead to a higher probability of success during fabrication.

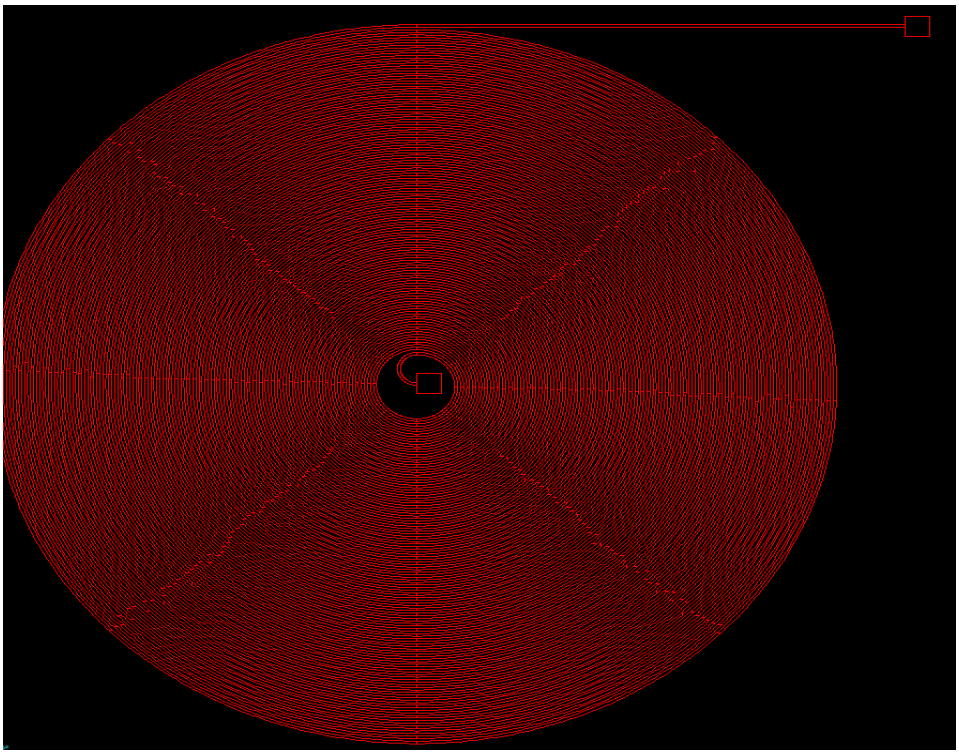

Figure 18: The spiral coil with a diameter of 7mm designed using CoventorWare

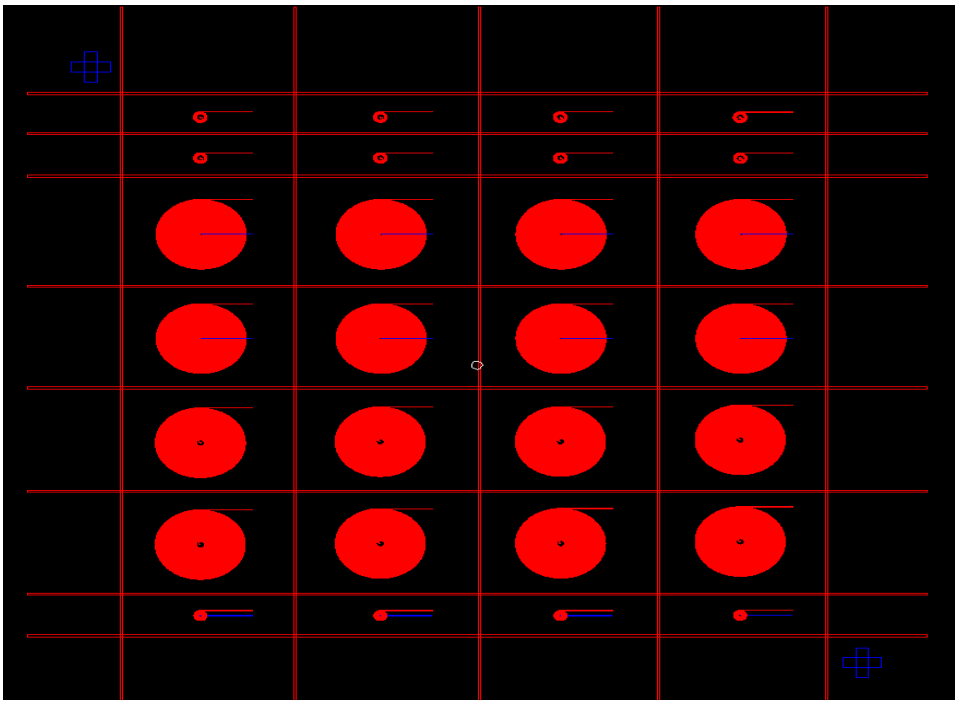

Figure 19: Layout of the final mask with the spiral coil designs

3 Fabrication Process

The designed mask containing the coil patterns was then sent for fabrication. This was used to make the micro-coils in the Nanotools laboratory. Initial fabrication procedure involved using Indium Tin Oxide (ITO) as the material to create the microcoils. The entire fabrication process is described below:

1. Deposition of ITO on a silicon wafer by using the Sputtering method. Ideally a biocompatible and flexible substrate such as Polydimethylsiloxane (PDMS) would be used instead of the Silicon (Si) wafer. As PDMS is also transparent, it is plausible to use to create a contact lens with PDMS and ITO coils which can be then placed on the eye. However the recipe for ITO deposition requires a substrate temperature of around 300^{o} C to improve conductivity which would damage the PDMS. Hence standard 4-inch Silicon wafers were utilized instead. The deposition was done with the Denton RF/DC Sputter system.
2. Photolithography which can be further divided into the following steps:
    - Spin coating the photoresist on the deposited ITO (Figure 20)
    - Exposing the photoresist to UV light through the coil mask using the EVG Aligner
    - Removing the exposed photoresist using developer and creating the coil patterns as a result (Figure 21)
3. Wet etching to remove the undesired parts of ITO to create the coils. This is done by using an etching solution which does not damage the photoresist and hence etches out all the ITO which is not part of the coil pattern (Figure 22).

4. The post-processing steps include dicing the wafer to separate the individual coils. Dicing involves slicing the wafer with automated diamond saws. Alignment markers were used to enable precise slicing of the wafers to separate the coils. There is an inherent risk of damaging the coil patterns from the wafer residue. These are then glued onto a PCB and wire bonding is used to make the electrical connections to the bonding pads on the coils.

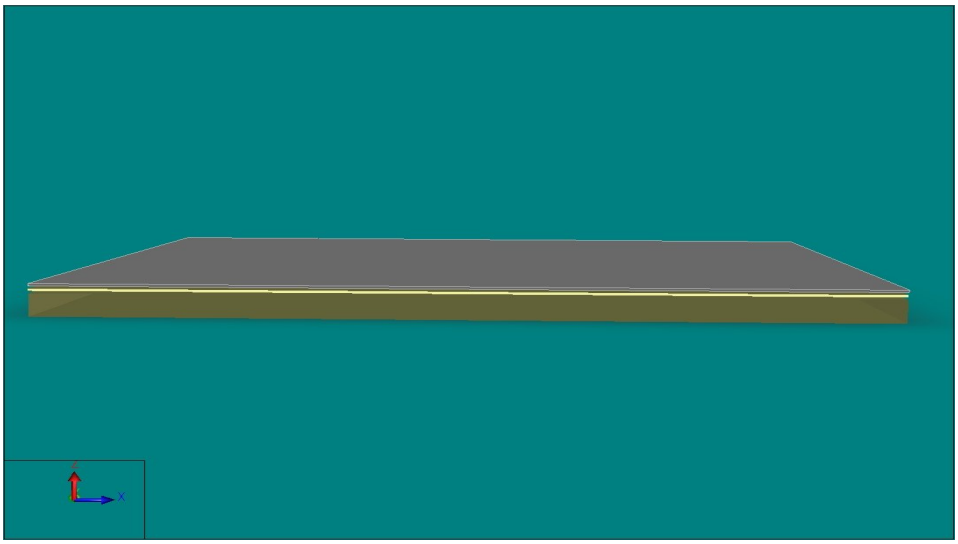

Figure 20: Silicon substrate with the deposited ITO and Photoresist (shown in grey color)

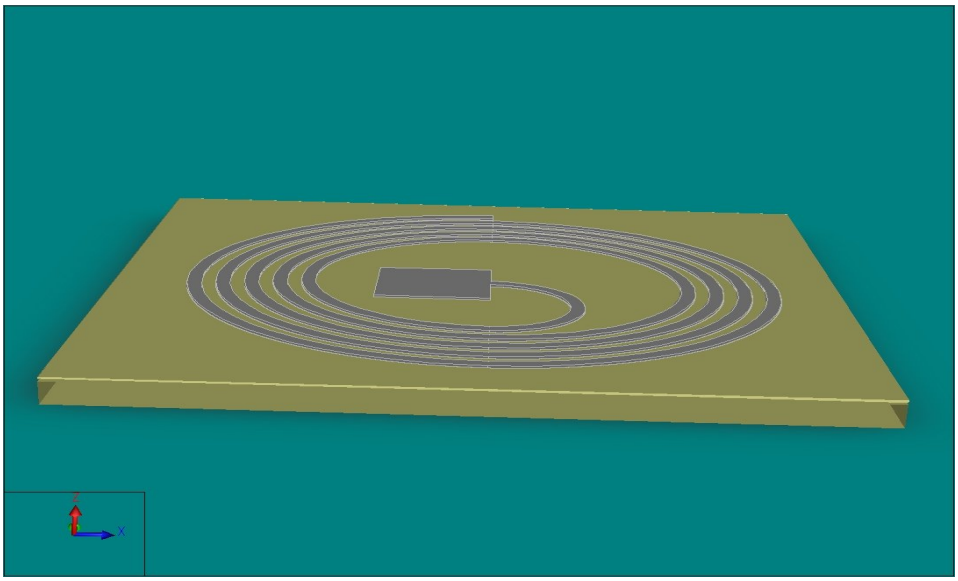

Figure 21: Coil pattern on the photoresist after development

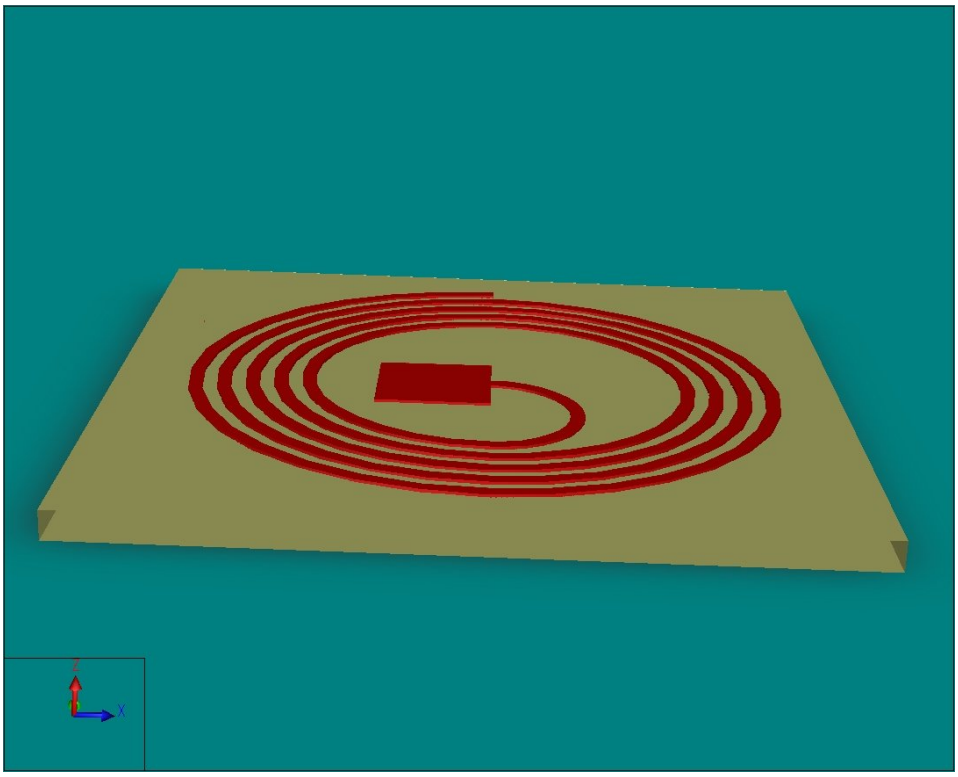

Figure 22: Silicon substrate with the final coil pattern using ITO

3.1 Micro-fabrication with ITO

As mentioned earlier, ITO was chosen as the material to fabricate the coils because of its optical transparency and electrical conductivity. However these properties depend heavily on the deposition process and the composition of the evaporation material used [30]. Both of these properties have to be balanced appropriately to achieve the desired results. For instance, the sheet resistance can be less than 10 Ohms/square with a visible transmission of greater 80% and this increases to more than 100 Ohms/square for a visible transmission of 90%. The main factors of the deposition process affecting the ITO properties are the partial pressure of oxygen, substrate temperature, rate of deposition and material composition [30]. An external laboratory Filmetrics Inc. had analyzed the ITO which was sputtered onto the wafer. It was reported that the ITO consisted of a sub-layer 338.5 nm thick with a refractive index (n) of 1.88 and a top layer 31.5 nm thick with n equal to 1.84. Hence, the deposited ITO was not uniform over its volume. We increased the deposition time to 3200 seconds from 2400 seconds in the recipe in order to increase the thickness of deposited ITO. The thickness of ITO was measured by using the Nanospec metrology tool which measures reflected light to determine film thicknesses based on interference effects. The thickness varied from 469.0 nm to 478.8 nm over the surface of wafer. The reason for the varying thickness can be attributed to the fact that Nanospec is mainly used for measuring thickness of photoresist and oxides. The measurement results for ITO are an approximation.

Step number 2 Photolithography followed the sputtering process. The coil patterns were created on the photoresist lying on top of the ITO layer. The next step was wet etching to remove the undesired parts of the ITO layer to create the desired microcoils. The Silicon wafer was cut into smaller parts in order to facilitate handling during the etching process. There are two common recipes for wet etching ITO as given in Table 3 [31].

Concentrations	**Etchants**	**Rate**
1:1	$HCl:H_2O$	8 angstroms/sec
1:1:10	$HF:H_2O_2:H_20$	125 angstroms/sec

Table 3: Wet chemical etching recipes for ITO

The first etching trials were conducted using the HF solution. With a rate of 125 angstroms/sec the ITO layer of thickness 4700 angstroms should take about 37.6 seconds to be etched. However the etching process did not produce the expected results even after several minutes. Different samples of the wafer were immersed in the HF solution but the etching of the ITO was not uniform over its area. Finally after 7-8 minutes the HF damaged the photoresist and the coil patterns. The whole deposition and etching process was repeated again with a new wafer to ensure that it was not an isolated incident but similar results were obtained (Figure 23).

The etching using the HCl solution also did not produce the desired results. This failure to etch the ITO with HF and HCl solutions can be attributed to the lack of uniformity mentioned earlier. The deposition process, chemical

properties of ITO and the materials used to make the etching solutions could have also lead to these results.

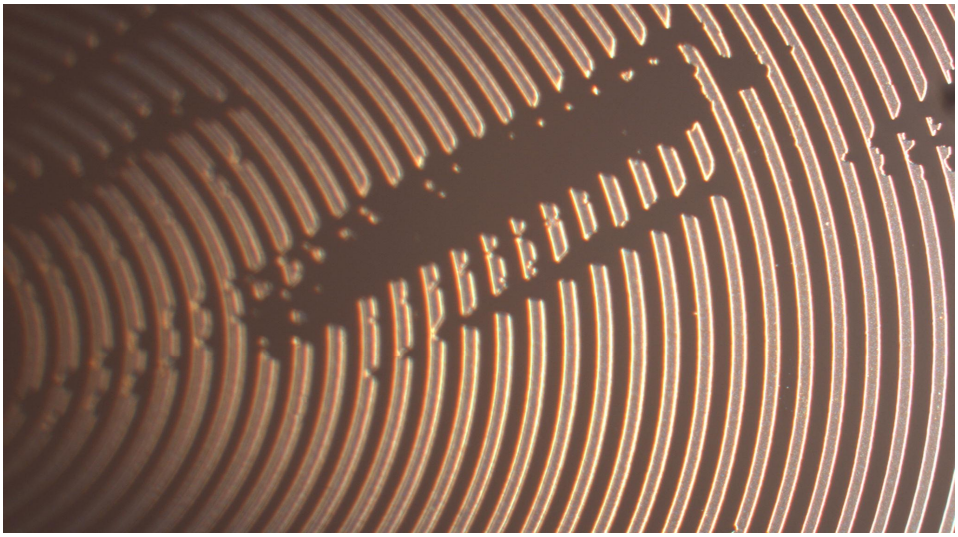

Figure 23: Picture of a damaged coil pattern using ITO after etching

As the wet etching of ITO did not provide the required patterns another technique called Lift-off process was attempted. The steps involved in this method are described below:

1. Photoresist was first deposited on a 4-inch Silicon wafer. It was then exposed to UV light and after the photolithography process the coil patterns were formed on the photoresist (figure 24).
2. ITO was then deposited on this wafer using Sputtering.
3. The wafer was then placed in Acetone for 10 minutes. The remaining photoresist was removed with the ITO deposited on top of it. The parts of ITO which were directly deposited on the substrate remained (figure 25).

Note that after the final processing step we obtain only the negative of the required coil pattern. This means that the final sample looked like ITO deposited on top of wafer with holes forming the microcoil pattern. However, this experiment showed that the lift-off process is capable of providing the required structures using ITO. The issue with this procedure is that it requires a negative photomask while we had only the positive one. A new negative mask for fabrication usually takes 3-4 weeks as it is sent to an external organization. Due to time constraints we decided to fabricate the microcoils with Aluminium instead. Another reason for using Al was its low resistivity which is around 28 nΩ.m compared to that of ITO measured to be 5 μΩ.m [32].

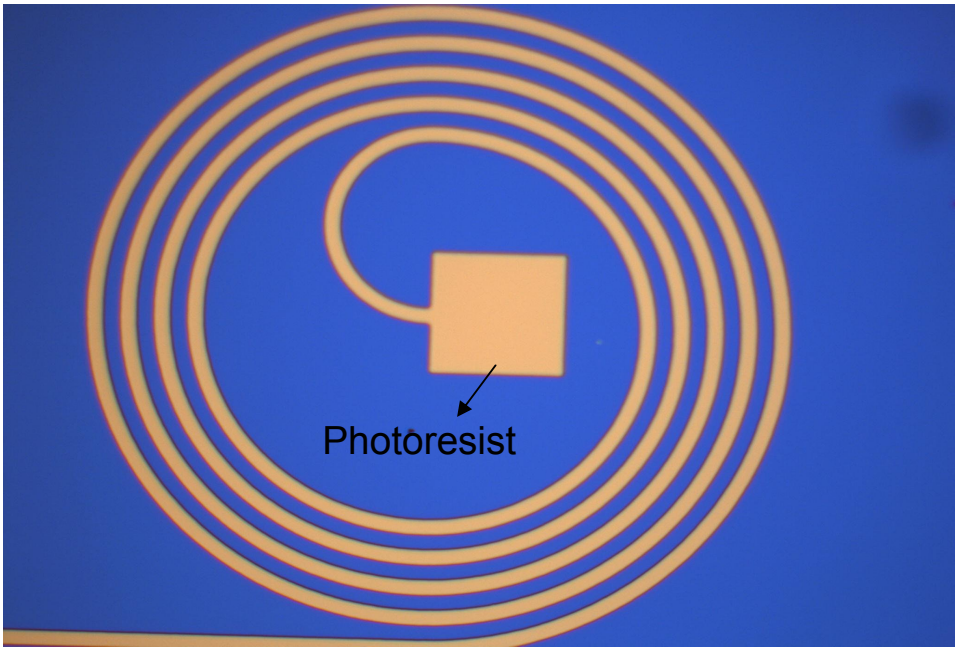

Figure 24: Photoresist with the coil pattern

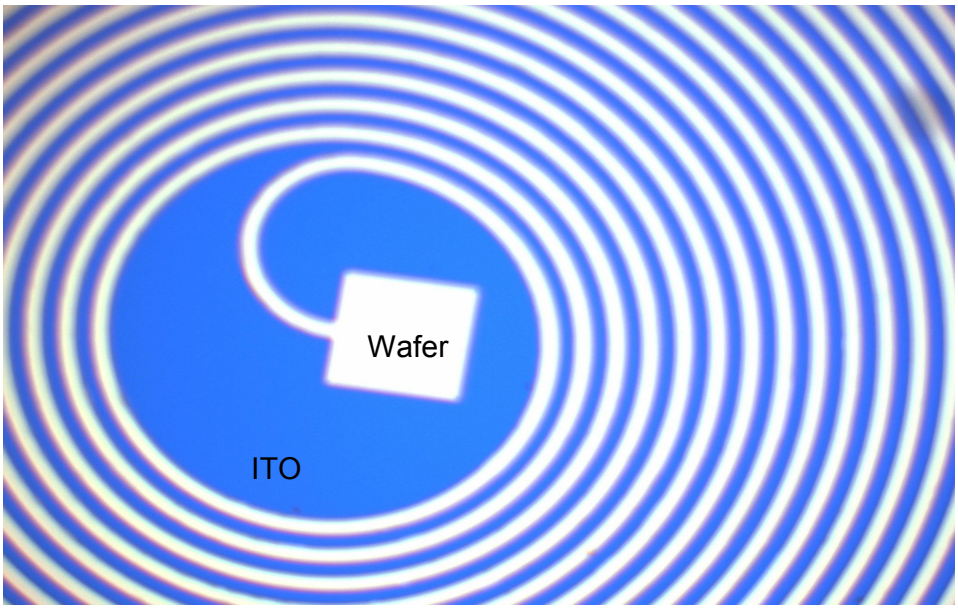

Figure 25: The final sample after the lift-off process

3.2 Micro-fabrication with Aluminium

As the use of ITO produced undesired results for the micro-coil fabrication, it was decided to fabricate the microcoils using Aluminium which is characterized by low resistivity and a standardized fabrication procedure. The same fabrication procedure as ITO was followed except for replacing the deposition of ITO with Aluminium and the wet etching was done using a commercial etchant. The coil-patterns were successfully obtained using Aluminium and they were then diced and wire bonded onto PCB (figures 26 and 27).

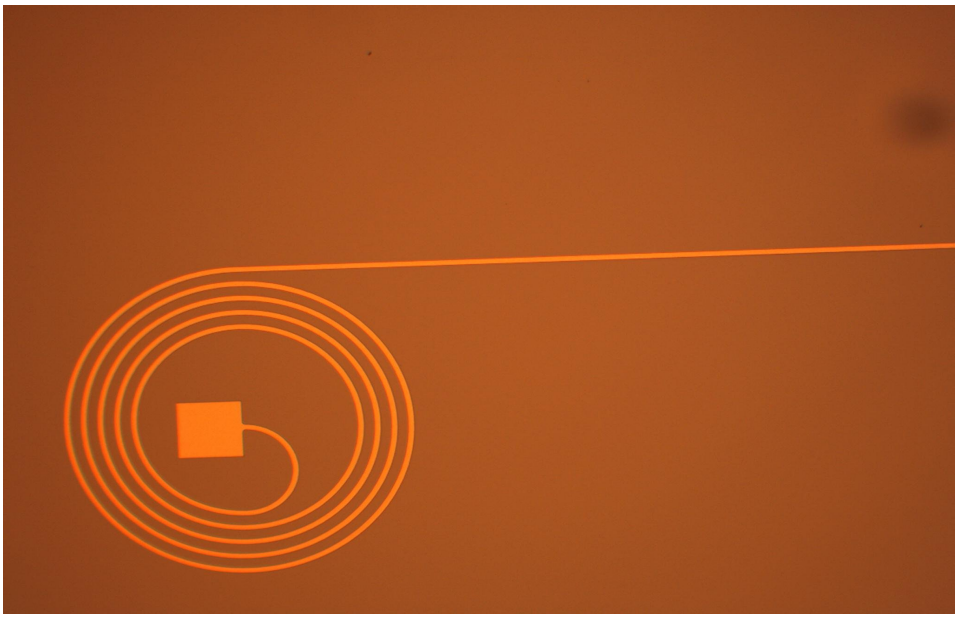

Figure 26: Picture of the 1 mm fabricated coil using Aluminium

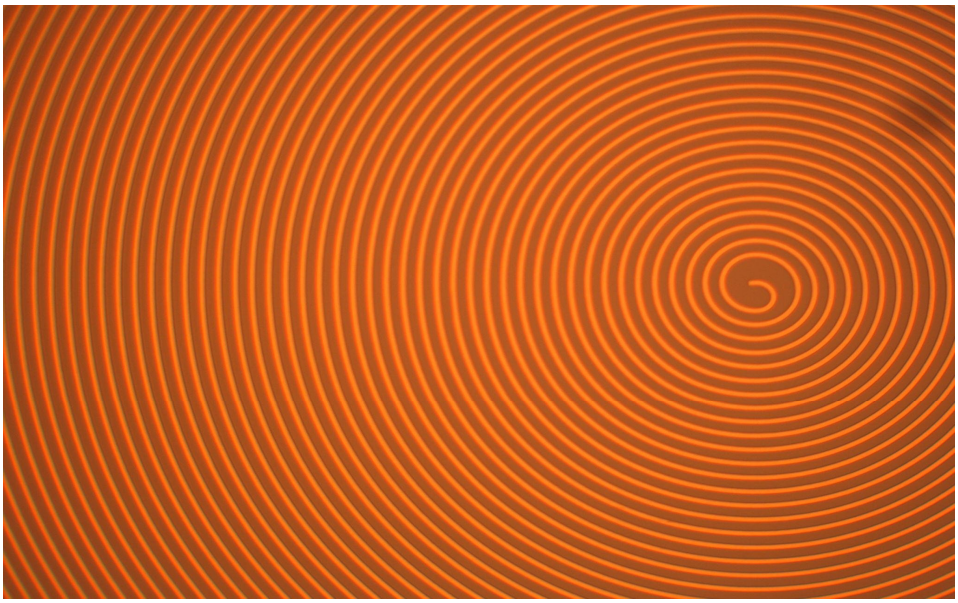

Figure 27: Picture of a fabricated coil using Aluminium

The attributes of the fabrication coils are as given below. As mentioned earlier, two sets of coils were made, C1 shown in Figure 28 and C2 shown in Figure 29.

C1 Diameter = 1 mm

Number of turns N = 10

Distance between tracks, d = 25 μm

Thickness of each track, t = 436 nm

Width of tracks, w = 25 μm

C2 Diameter = 7 mm

Number of turns N = 70

Distance between tracks, d = 25 μm

Thickness of each track, t = 436 nm

Width of tracks, w = 25 μm

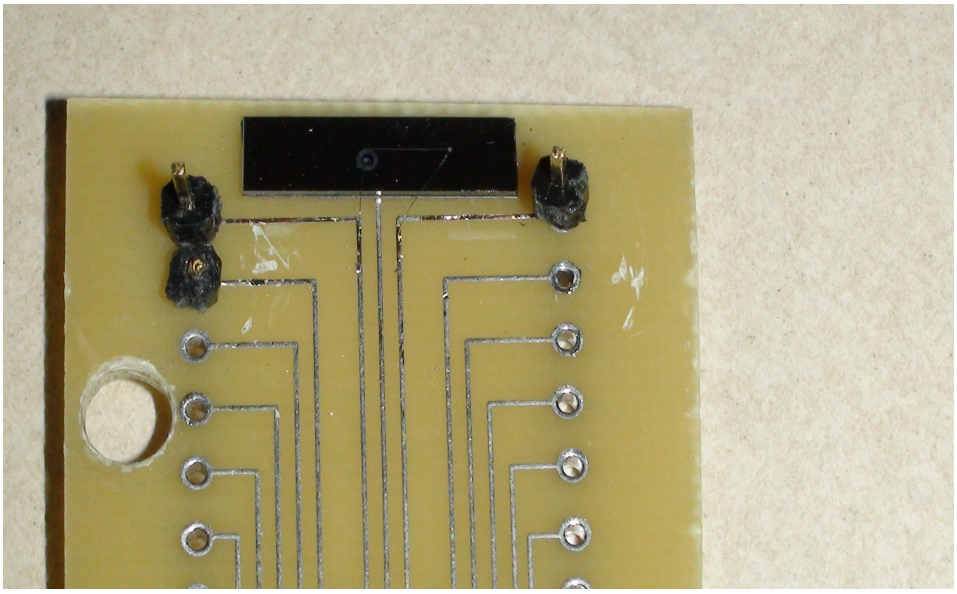

Figure 28: Picture of a fabricated 1 mm after wire bonding on the PCB

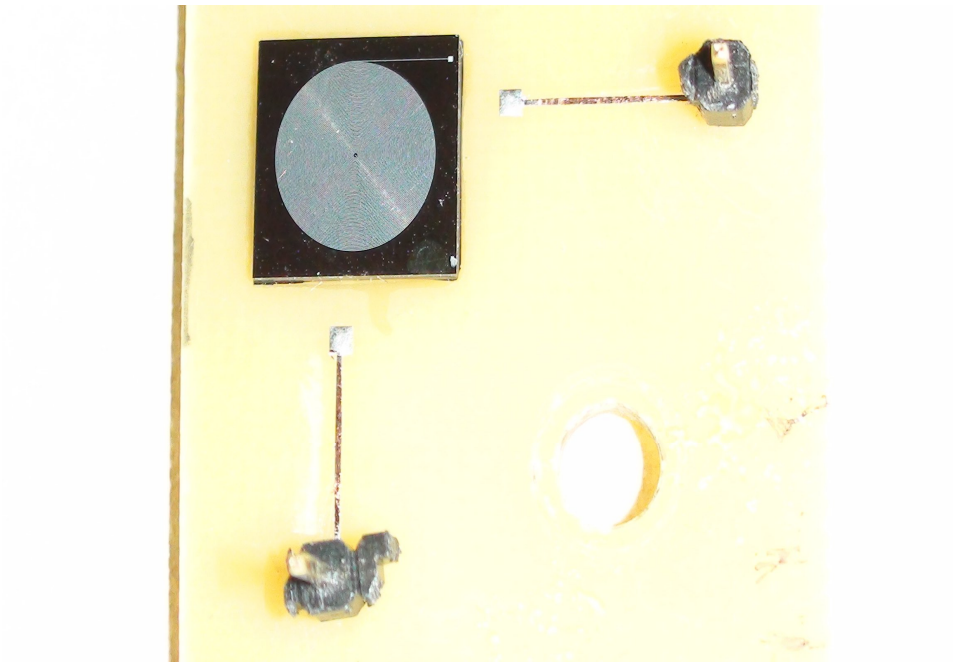

Figure 29: Picture of the fabricated 7 mm coil on the PCB

4 Testing and Measurement results using Aluminium microcoils

After the fabrication and post-processing procedures the next step was to evaluate the feasibility of the microcoils for the purpose of movement detection. For this purpose, only two coils were used at a time for experimentation. The reason for this was to simplify the system, to prove the concept and to identify potential problems. So, initially one coil was used as the primary coil to generate the magnetic field and the other magnetically coupled coil as secondary used to measure any relative movements.

4.1 Configuration of the Testing Apparatus

The current in the primary coil was produced using a function generator (Tabor Electronics WW2572 A) since it was required to produce an alternating magnetic field. The primary coil was then attached onto a post using screws and it was connected to the function generator using a regular coaxial cable with crocodile clip ends (figure 30). The secondary coil was attached to a stereotax using screws as well. The stereotax has the ability to move the coil vertically and also laterally. As we needed to acquire the voltage induced in the secondary coil it was connected to an oscilloscope via a preamplifier. The preamplifier Stanford Research systems Model-SR560, contained a band-pass filter and an amplifier. The oscilloscope used was Tektronix model TDS-3024B. The cut-off frequencies for the band-pass filter and the amplification gain could be varied depending on the desired signal.

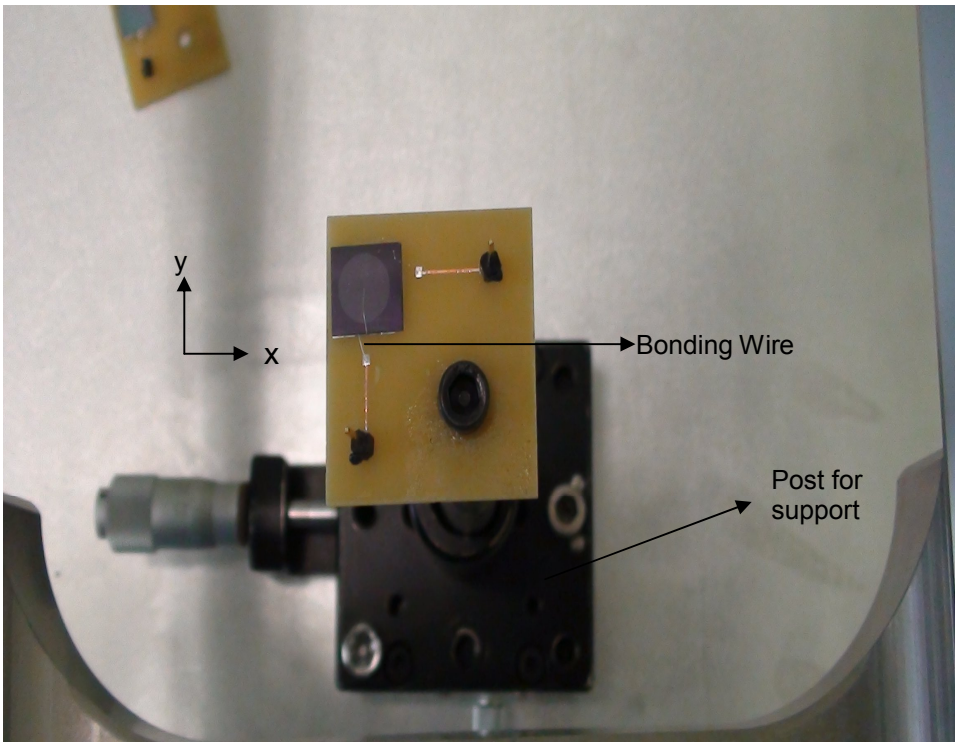

Figure 30: Picture of the primary coil attached to its support

A simplified block diagram explaining the system configuration can be seen in figure 31. The first experiments were conducted with the 1 mm coils (C1) as both primary and secondary coils. The voltage from the function generator across the coil was in the form of $V = V_O Sin(\omega t)$ where V_O is the amplitude and ω is $2\Pi f$. The signal applied from the function generator had the following attributes:

Voltage Amplitude = 2.8 V

Frequency = 500 kHz

DC Offset = 0 V

The cut-off frequencies in the preamplifier were set to 30 kHz and 1 MHz and the gain was set to 1000. The coil setup, coordinate axis and the stereotax is shown in figure 32.

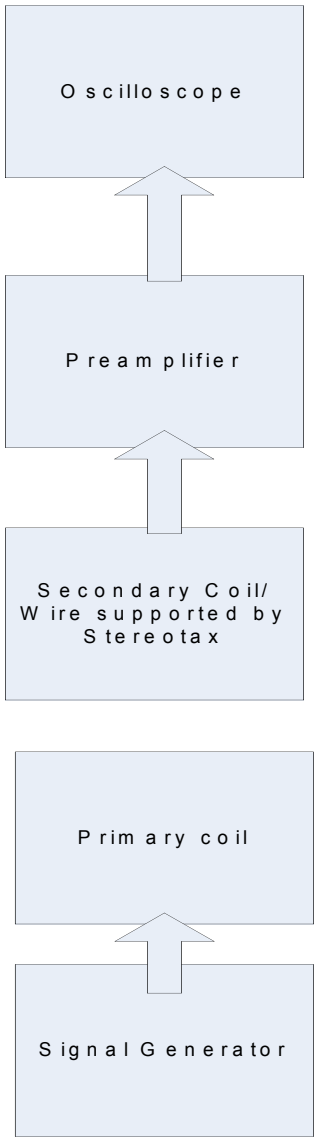

Figure 31: A block diagram of configuration of the testing apparatus

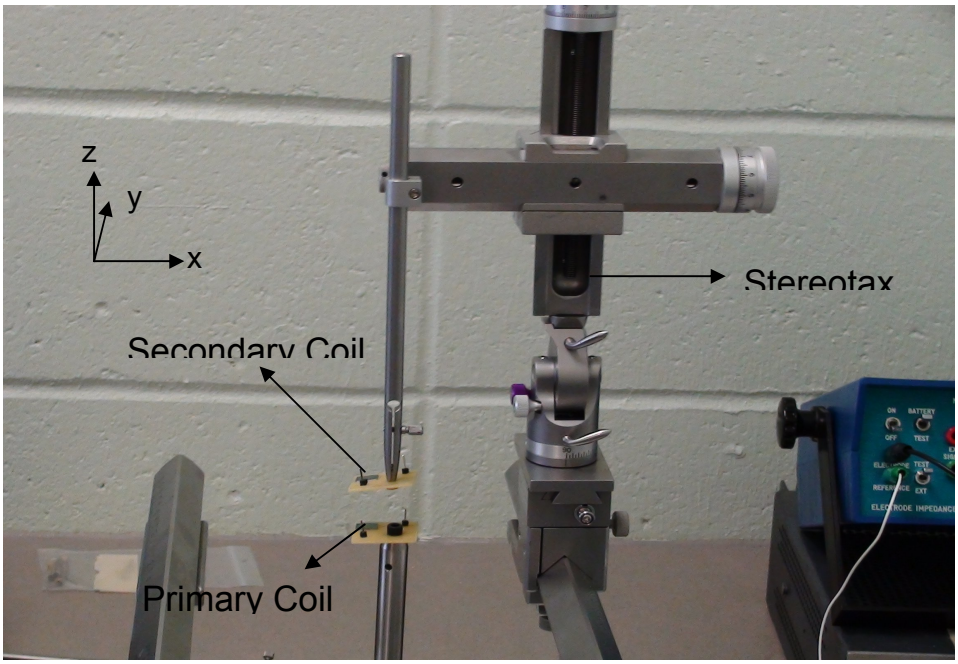

Figure 32: Picture of the coil configuration showing the apparatus used for measurements

4.2 Measurement Results and Discussion

It was noted that the induced voltage amplitude in the secondary coil was around 649 mV even when the distance between the primary and secondary coil was around 7-8 cm. This was unexpected as the induced voltage in the secondary coil should be negligible unless the primary coil was in very close proximity such as a few millimetres away. The induced voltage was observed because the clip ends of the coaxial cable are not magnetically shielded and hence induced a voltage in the cables connected to the secondary coil. The magnetic field generated by these cables was much stronger than the one from the primary coil because of their larger dimensions. As a result, their effect would dominate the inductive coupling between the coils. To confirm this hypothesis, the coils were removed altogether from the system and the induced voltage could still be observed. Hence it was required to ensure that the

connecting cables to the coils were shielded and did not contribute to the inductive link. This was done by using coaxial cables with BNC connectors at both ends. Appropriate male/female connectors were used to make the required connections to the coils. However, this provided another hindrance in the system configuration as the new connectors at the cable ends were found to be cumbersome to be connected to the PCB. This was noticed especially for the secondary coil on the stereotax. Furthermore, the 1 mm coils were not able to form a strong inductive link irrespective of the voltage amplitude and frequency of the signal in the primary coil. The input voltage was varied between 1 – 10 V peak but the induced voltage in the secondary coil was negligible. It was then decided to use the coil C2 with diameter of 7 mm instead as the primary coil. The secondary coil was replaced by a thin strip of copper wire around 3 cm long, this was done as the PCB containing the coil could not be attached to the stereotax in a relatively stable fashion. The cable end connecting to the preamplifier also added to the instability. It is of prime importance to be able to correctly identify the location of each coil in order to measure any relative displacement. Hence, if the PCB with the secondary coil is not attached securely to the stereotax then the coil orientation could easily change due to the slightest of mechanical perturbations for example while making connections with the coaxial cable. A strip of copper wire was easily attached to the stereotax and its position was found to be stable. This was a satisfactory replacement in order to the study the inductive link with the primary coil.

The alternating magnetic field from the primary coil induced an alternating voltage across the ends of the wire. This induced voltage was amplified by the preamplifier and measured from the oscilloscope. The wire was then displaced using the knobs on the stereotax and the resulting change in induced voltage was noted. This process was repeated for different starting positions of the wire to study their effects on the resolution and noise in the signal. The primary coil was kept stationary through out the experiments. The objective was to find a correlation between the induced voltage in the wire with respect to its change in position.

The first experiments were conducted by just moving the wire vertically. If we assume that the primary coil lies in the x-y plane then the wire was moved along the z-axis (figure 32). The centre of the coil is considered to be the origin (x = 0, y = 0, z = 0). The wire was placed directly above the coil, that is x and y displacements were zero. The input signal from the function generator applied to the primary coil can be represented as $V_O Sin(\omega t)$ where $V_O = 10$ V, $\omega = 2\Pi f$ and f = 500 kHz.

Figure 33 shows a graph between the induced voltage and the distance between primary coil and the wire. The data used to create the graph is shown in Table 4 for reference. As expected the induced voltage increases considerably when distance between the wire and coil is decreased.

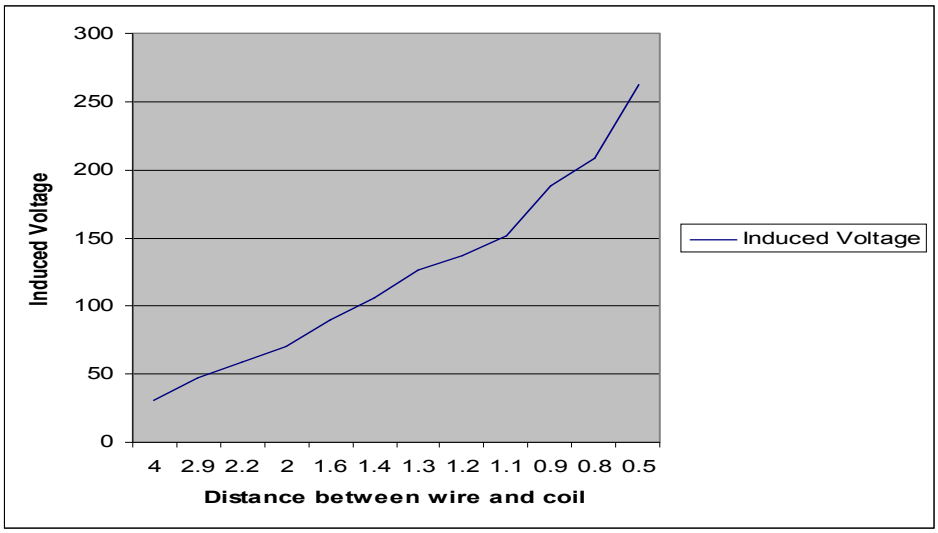

Figure 33: Induced voltage in the wire versus its distance from the primary coil

Distance of wire from the coil in vertical z-axis (cm) (x = 0, y = 0)	**Induced voltage (mV) after amplification (Gain = 1000)**
4	27.8-33
2.9	41.6-53.6
2.2	58.4
2	70.8
1.6	89.6-90.4
1.4	106
1.3	126
1.2	135-138
1.1	151
0.9	187-189
0.8	208
0.5	261-264

Table 4: Induced voltage in the wire with respect to its distance from the primary coil

The signal read from the oscilloscope can be seen in figures 34, 35, 36 and 37 for different positions of the wire.

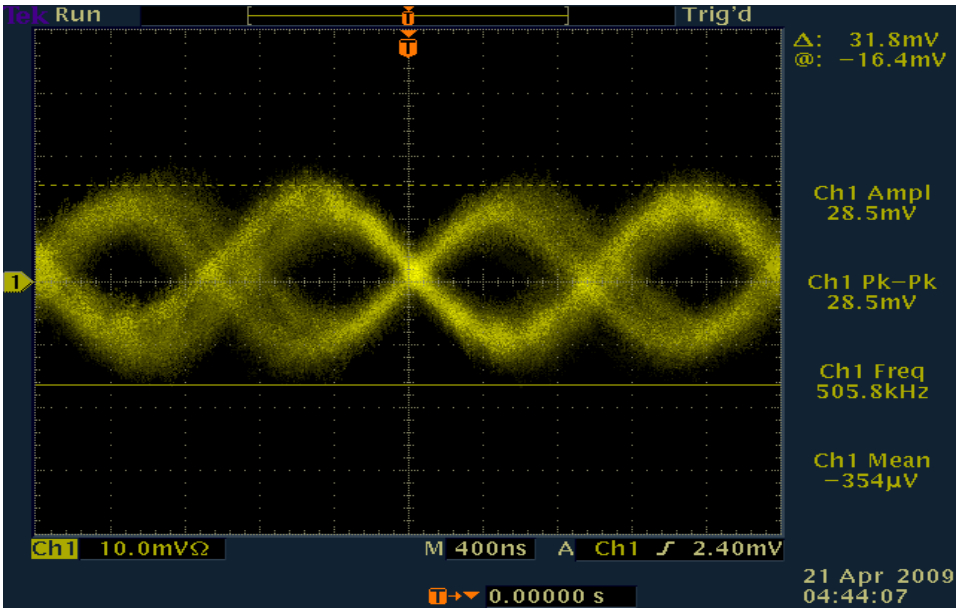

Figure 34: Induced voltage in the wire when distance from primary coil = 4 cm

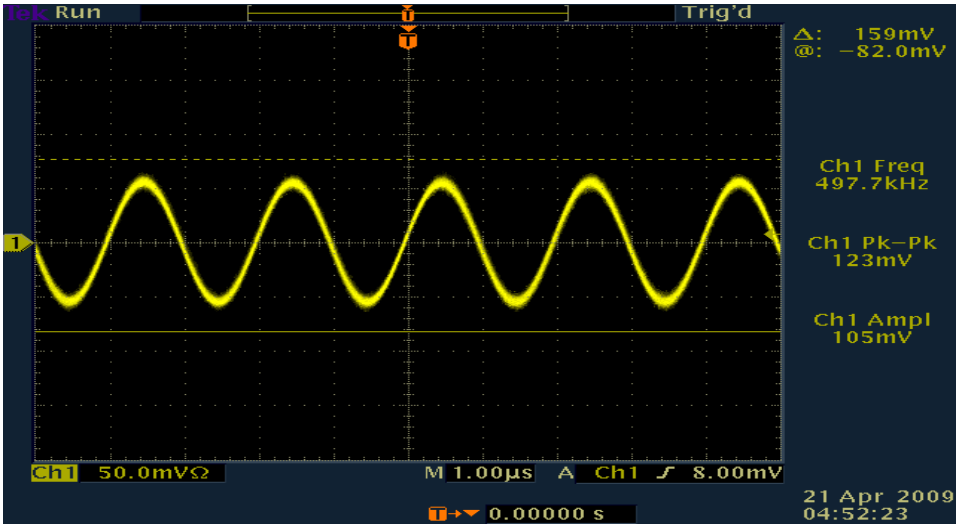

Figure 35: Induced voltage in the wire when distance from primary coil = 1.4 cm

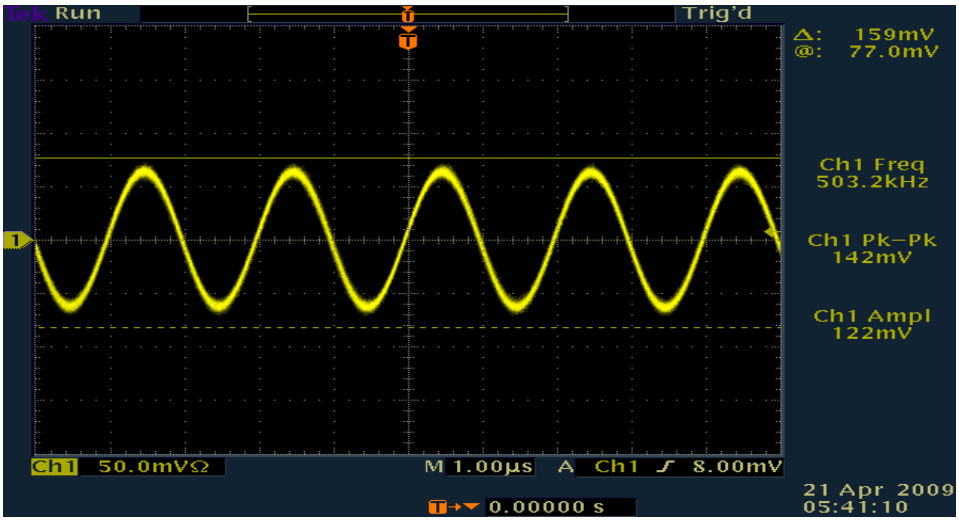

Figure 36: Induced voltage in the wire when distance from primary coil = 1.2 cm

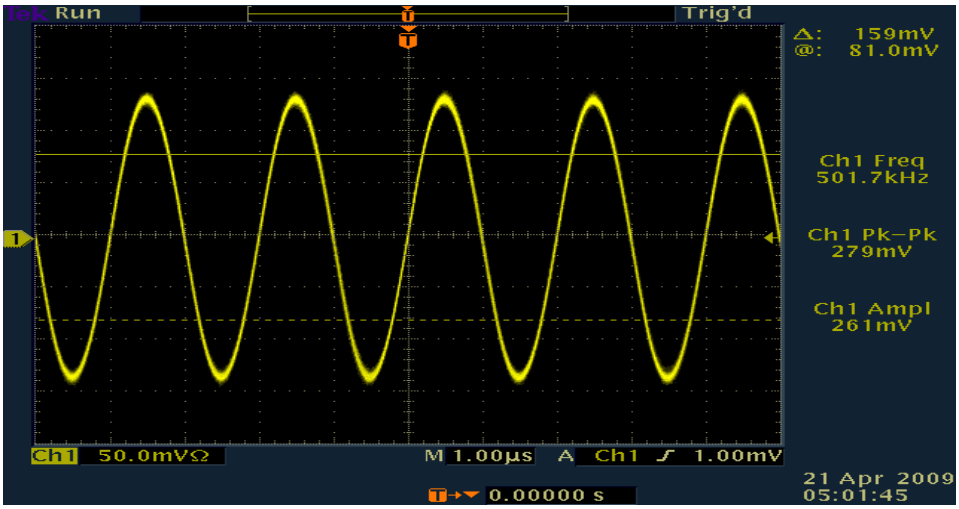

Figure 37: Induced voltage in the wire when distance from primary coil = 0.5 cm

As can be seen, the induced voltage signal deteriorates at increased distances from the coil.

For the purpose of the project we need to analyze the change in induced voltage when there is lateral displacement of the wire, that is along the x and y axis (figure 32). The lateral displacement is a more accurate representation of

the eye movement. Here we assume that the wire and the eye lie in the x-y plane. The primary coil is placed at a certain distance z, directly in front of the eye also in the x-y plane. This distance z will have to be fixed for accurate measurements. Hence, we need to find the appropriate distance z which will give the desired results. If this distance is too large then the induced voltage signal is poor and unreliable for any useful information. However, if this distance is too small then the coil would lie very close to the eye and obstruct the vision. From the results given above the ideal distance z would be between 0.5 and 1.2 cm.

The next step in testing was to study the induced voltage in the wire for lateral displacements. This was done by fixating the wire at a distance z = 0.6 cm above the coil and then using the knobs on the stereotax to move it along the y axis. The minimum displacement possible for the wire with this system was 10 μm. The following table 5 shows different values of induced voltage observed while the wire is displaced along the y-axis.

Change in position (μm) (vertical distance z = 0.6 cm)	**Induced voltage in Wire in mV (after amplification)**
20	444 - 446.5
20	444 – 446.8
20	446.2 – 448.4
50	454 – 456.8
20	508.4 – 509.0
20 (near centre)	536 – 538.2
20	512 – 517.8
20	508 – 511.4

Table 5: Induced voltage in the wire during lateral displacement along the y-axis

We need to notice two important facts from the data above. First, the average resolution of this particular system is around 20 μm - 40 μm. Second, the change in induced voltage increases significantly when the wire is near the centre of the coil. This can be attributed to the magnetic field distribution of the coil with the lateral deviation.

Woytasik *et al* [33] fabricated copper planar coils for applications in magnetic actuation. Their reports confirm that the magnetic field reaches its peak at the centre of the coil and falls rapidly upon displacement. As the induced voltage is directly related to the magnetic field the induced voltage also changes at the same rate. It was also reported in their study that with an increase in distance from the coil the magnetic field becomes more uniform across the lateral

deviation. This is undesirable as it would become more difficult to examine changes in induced voltages. This phenomenon can be observed from the data in Table 6 as the resolution decreases with an increase in distance between the primary coil and the secondary coil/wire.

Distance between microcoil and wire (in cm) z direction	**Displacement of wire (µm)**	**Change in Induced voltage (mV)**
0.4 – 0.5	20	56
0.6	20	28
1	20	8
1.2	20	5
2	20	3

Table 6: Resolution of the coil/wire configuration at different distances

The results discussed so far show that an inductive link using the fabricated coil system can be used to detect displacement of the secondary coil/wire. We decided to replace the secondary wire with a micro-probe wire to see the differences in induced voltage.

Induced Voltage using copper wire 3 cm long	**Induced Voltage using micro-probe wire**	**Position of the copper wire and the micro-probe with respect to the primary coil**
434 – 438 mV	374-378 mV	z = 0.6 cm

Table 7: Comparison of induced voltage using the copper wire with the micro-probe wire

Both the wires were of approximately the same length and placed at the same location with respect to the primary coil. The data shown in the measurement results was recorded using the copper wire as the micro-probe wire and the secondary coil could not be connected securely to the stereotax and the coaxial cables. However, we can see that the micro-probe wire can also be used in the inductive link with a lower value of induced voltage. A wire with thickness in micrometers could be placed on the eye with ease when compared to the regular copper wire.

5 Conclusion

While there are a number of eye tracking techniques available there is a vast scope for improvement in terms of miniaturizing the setup. In this thesis we proposed to use MEMS technology to fabricate microcoils for application in eye movement measurement. The design and physical parameters of the proposed microcoils were discussed. Simulations pertaining to the electromagnetic effect and the fabrication procedure of the microcoils using Indium Tin Oxide (ITO) and Aluminium were presented and analyzed. Finally the measurement results using these coils were shown. We found that the inductive link comprising of the coils can be used to measure displacements. The resolution however is not fixed and depends on the configuration of the coil system. The resolution was calculated to be around 20-40 μm on the plane of the coil and it increases near the centre of the coil.

There is a potential for using this system for eye movement measurements but further investigation is required. First, the whole system has to be characterized and stabilized by creating a customized testing environment. These include supports, connections for the coils and the other testing apparatus. The coil system should be tested in an environment which simulates eye movements such as the velocity of the eye, saccades. Furthermore, the possibility of using ITO can be explored as this can lead to a transparent coil system. The first task would be to find the right balance between the desired optical transparency and the electrical conductivity. This can be achieved by choosing the appropriate deposition and fabrication process. We were able to produce the coil patterns using ITO employing the lift-off process. However,

the wire bonding process to connect the ITO coils would not be a straightforward as the bonding wires are usually made of conventional metals such as Gold or Aluminium. It is critical for the coil system to provide consistent results while able to withstand the mechanical disturbances arising from the experiments. So the feasibility of using ITO coils in an experimental environment would have to be tested for the purpose of measuring eye movements.

References

[1] Duchowski, Andrew T. 2003. *Eye tracking methodology, Theory and Practice*. Springer-Verlag London Limited

[2] Snodderly, M.D., Igor Kagan and Moshe Gur. 2001. Selective activation of visual cortex neurons by fixational eye movements: Implications for neural coding. *Visual Neuroscience*. 18: 259–277

[3] Asaad, W.F., Gregor Rainer and Earl K. Miller. 2000. Task-Specific Neural Activity in the Primate Prefrontal Cortex. *The Journal of Neurophysiology*. 84: 451-459

[4] Rayner, K. 1998. Eye movements in Reading and Information Processing: 20 Years of Research. *Psychological Bulletin*. 124(3): 372-422

[5] Leigh, R. John, and David S. Zee. 2006. *The Neurology of Eye Movements*. Oxford University Press

[6] Rucker, JC., BE Shapiro, YH Han, AN Kumar, S Garbutt, EL Keller and RJ Leigh. 2004. Neuro-ophthalmology of late-onset Tay-Sachs disease (LOTS). *Neurology*. 63(10):1918-26

[7] Tanaka, M., and Stephen G. Lisberger. 2001. Regulation of the gain of visually guided smooth-pursuit eye movements by frontal cortex. *Nature*. 409:191-194

[8] Jacob, R. J. 1990. What You Look at is What You Get: Eye Movement-Based Interaction Techniques. Human Factors in Computing Systems: CHI ’90 Conference Proceedings. 11-18

[9] Methods of Measuring Eye Movements. University of Liverpool. http://www.liv.ac.uk/~pcknox/teaching/Eymovs/emeth.htm

[10] The McGill Physiology Virtual Lab. Biological Signals Acquisition. http://www.medicine.mcgill.ca/physio/vlab/Other_exps/EOG/eogintro_n.htm

[11] METROVISION. 4 rue des Platanes, 59840 Pérenchies, France. www.metrovision.fr

[12] Glenstrup, J. A., and Theo Engell-Nielsen. 1995. Eye Controlled Media:

Present and Future State. Thesis for the Partial Fulfillment of the Requirements for a Bachelor's Degree in Information Psychology at the Laboratory of Psychology, University of Copenhagen.

[13] Robinson, D.A. 1963. A Method of Measuring Eye Movement Using a Scleral Search Coil in a Magnetic Field. *IEEE Transactions on Bio-Medical Electronics*. 10:137-145

[14] Sprenger, A., B. Neppert, S. Köster, S. Gais, D. Kömpf, C. Helmchen and H. Kimmi. 2008. Long-term eye movement recordings with a scleral search coil-eyelid protection device allow new applications. *Clinical Neurophysiology*. 120 (1):e42-e43

[15] Schmitt, K.U., Markus H. Muser, Christian Lanz, Felix Walz and Urs Schwarz. 2006. Comparing eye movements recorded by search coil and infrared eye tracking. *Journal of Clinical Monitoring and Computing*. (2007) 21:49–53

[16] Van der Geest, JN., and MA Frens. 2002. Recording eye movements with video-oculography and search coils: a direct comparison of two methods. *Journal of Neuroscience Methods 114* (2), 185-195.

[17] Träisk, F., R. Bolzani and J. Ygge. 2004. A comparison between the magnetic scleral search coil and infrared reflection methods for saccadic eye movement analysis. *Graefe's Archive for Clinical and Experimental Ophthalmology*. 243: 791 – 797

[18] Fuchs, A.F., and David A. Robinson. 1966. A method for measuring horizontal and vertical eye movement chronically in the monkey. *Journal of Applied Physiology*. 21: 1068-1070

[19] Collewijn, H., F. van der Mark and T.C. Jansen. 1975. Precise recording of human eye movements. *Vision Research*. 15:447-450

[20] Judge, S., B. Richmond, and F. Chu.1980. Implantation of magnetic search coils for measurement of eye position: An improved method. *Vision Research*. 20 (6):535-538.

[21] Remmel, Ronald S. 1984. An inexpensive eye movement monitor using the Scleral Search coil technique. *IEEE Transactions on Bio-Medical Engineering*. 31:388-390

[22] Kenyon, Robert V. 1985. A soft contact lens search coil for measuring eye movements. *Vision Research* 25:1629-1633

[23] Kim, Keun Y., Seung Yup Lee and Hee Chan Kim. 2004. A Wireless Measurement System for Three-dimensional Ocular Movement Using the Magnetic Contact Lens Sensing Technique. Proceedings of the 26th Annual International Conference of the IEEE EMBS. San Francisco, CA, USA • September 1-5, 2004

[24] Reulen, J. P. H. and L. Bakker. 1982. The measurement of Eye Movement using Double Magnetic Induction. *IEEE Transactions on Biomedical Engineering*.29 (11): 740-744

[25] Malpeli, Joseph G. 1998. Measuring eye position with the double magnetic induction method. *Journal of Neuroscience Methods*. 86:55–61

[26] Bremen, P., Robert F. Van der Willigen, and A. John Van Opstal. 2007. Applying Double Magnetic Induction to Measure two-dimensional Head-Unrestrained gaze shifts in human subjects. *Journal of Neurophysiology*. 98: 3759-3769

[27] Ogorodnikov, D., Sergey Tarasenko, Sergei Yakushin, Bernard Cohen, and Theodore Raphan. 2006. Head fixed field coil system for measuring eye movements in freely moving monkeys. Proceedings of the 28th IEEE EMBS Annual International Conference. New York City, USA, Aug 30 – Sept 3, 2006. 1:5567-70

[28] Ramadan, Q., Victor Samper, Daniel Poenar and Chen Yu. 2004. On-chip micro-electromagnets for magnetic-based bio-molecules separation. *Journal of Magnetism and Magnetic Materials.* 281:150-172

[29] Varadan, Vijay K., K.J. Vinoy and K.A. Jose. 2002. *RF MEMS and Their Applications.* John Wiley & Sons LTD.

[30] Cerac Incorporated Technical Publications. ITO, TIN-DOPED INDIUM OXIDE FOR OPTICAL COATING. http://www.cerac.com/pubs/proddata/ito.htm

[31] Department of Electrical and Computer Engineering. Brigham Young University. Wet Chemical Etching of Metals and Semiconductors. http://www.ee.byu.edu/cleanroom/wet_etch.phtml

[32] Webpage by Glenn Elert. The Physics Hypertextbook An Encyclopedia of Scientific Essays. Resistivity of Aluminium. http://hypertextbook.com/facts/2004/ValPolyakov.shtml

[33] Woytasik, M., Johan Moulin, Emile Martincic, Ann-Lise Coutrot, Elisabeth Dufour-Gergam. 2007. Copper planar microcoils applied to magnetic actuation. *Microsystems Technology*. 14:951-956

[34] Buquet, C., Jacques Charlier, Guy Dhelin, Sylvie Toucas, Maurice Quere, Isabelle Moati. 1992. Photo-oculography: A New Method For Eye Movements Study, Interest In Ophthalmological And Extra Pyramidal Neurological Diseases. *Engineering in Medicine and Biology Society*. Proceedings of the Annual International Conference of the IEEE. 14: 1555-1556